Benchmarking the seismic assessment of unreinforced masonry buildings from a blind prediction test

F. Parisse [a,*], S. Cattari [b], R. Marques [a], P.B. Lourenço [a], G. Magenes [c,j], K. Beyer [d], B. Calderoni [e], G. Camata [f], E.A. Cordasco [e], M.A. Erberik [g], C. İçel [g], M. Karakaya [h], D. Malomo [i], C.F. Manzini [j], C. Marano [f], F. Messali [k], G. Occhipinti [l], B. Pantò [m], Ö. Saygılı [n], M. Sousamli [k]

[a] *ISISE, Department of Civil Engineering, University of Minho, Guimarães, Portugal*
[b] *Department of Civil, Chemical and Environmental Engineering (DICCA), University of Genova, Genova, Italy*
[c] *Department of Civil Engineering and Architecture (DICAr), University of Pavia, Pavia, Italy*
[d] *Earthquake Engineering and Structural Dynamics Laboratory (EESD), School of Architecture, Civil and Environmental Engineering (ENAC), École Polytechnique Fédérale de Lausanne (EPFL), EPFL ENAC IIC EESD, Lausanne, Switzerland*
[e] *Department of Structures for Engineering and Architecture, University of Napoli Federico II, Napoli, Italy*
[f] *Department of Engineering and Geology, University G. D'Annunzio of Chieti-Pescara, Chieti, Italy*
[g] *Department of Civil Engineering, Middle East Technical University, Ankara, Turkey*
[h] *Department of Earthquake Engineering, Kandilli Observatory and Earthquake Research Institute, Boğaziçi University, Istanbul, Turkey*
[i] *Department of Civil Engineering and Applied Mechanics, McGill University, Montréal, QC, Canada*
[j] *European Centre for Training and Research in Earthquake Engineering (EUCENTRE), Pavia, Italy*
[k] *Faculty of Civil Engineering and Geosciences, Delft University of Technology, Delft, the Netherlands*
[l] *Institute of Environmental Geology and Geoengineering, Italian National Research Council (CNR), Rome, Italy*
[m] *Department of Civil and Environmental Engineering, Imperial College London, London, United Kingdom*
[n] *Department of Civil Engineering, Yeditepe University, Istanbul, Turkey*

ARTICLE INFO

ABSTRACT

This paper presents a benchmark exercise for the seismic assessment of unreinforced masonry (URM) buildings as a follow-up of a blind prediction test organized in the context of the European Conference of Earthquake Engineering Series. The blind prediction exercise was aimed at better defining the open issues in current procedures for modeling and performing seismic analysis of URM buildings, by highlighting the uncertainty that can influence the results. This work presents an overview of the approaches used by different research teams and the scope of predictions. The benchmark structure was a three-story building with traditional European architecture from which two Cases were considered: A) stone masonry walls and flexible horizontal diaphragms and B) brick masonry walls and rigid horizontal diaphragms. A wide range of approaches was used by the participating teams concerning modeling strategies, methods of analysis and criteria for the attainment of limit states, which are here addressed as potential sources for the dispersion of predictions. The results were compared in terms of capacity curves, predicted failure mechanisms compatible with the fulfillment of limit states of near collapse and damage limitation, and related minimum values of peak ground acceleration (PGA). The results show an overall good agreement for damage patterns and collapse mechanisms in both benchmark structures, presenting some differences in the type of failure mode and its extent. However, the scatter of predicted capacity curves and critical PGAs is very high, especially for the Case with brick masonry and rigid diaphragms, indicating that clearer procedures in the building codes are required for professionals.

1. Introduction

The safety assessment of existing structures is a process requiring understanding at structural and material levels, including collecting data about geometrical configuration, construction process and details, as well as about mechanical properties of materials. In existing buildings, data collection is not always viable or economically affordable, at least in depth, and it is characterized by important uncertainty meaning

---

that suitable assumptions are required to perform the assessment. This issue is more evident for non-engineered structures, such as many URM buildings, because of high nonlinearity and variability of material properties, phased construction, uncertainty in connection between elements and lack of capacity design principles [1]. Despite this context, attempts have been made to standardize such a process and consequently limiting the arbitrariness of assumptions [2]. Still, the process may result in very different evaluations even when starting from the same initial information, because it is much dependent on modeling assumptions and methods of analysis, which require the judgment and experience of the professionals involved. After obtaining the structural response, the dispersion is likely to increase due to different criteria in defining the attainment of limit states conceptually outlined by standards (such as the Near Collapse – NC – and Damage Limitation – DL – proposed in Eurocode 8 Part 3 [3]). Seismic vulnerability predictions can be scattered even for code-based designed modern URM buildings, depending on the method of analysis, as shown in [4,5], in great extent due to the fact that the nonlinearity of the response needs to be taken into account.

A comprehensive and reliable prediction of the seismic capacity of existing URM structures should consider the behavior at both global and local levels, which means including the different failure mechanisms that may occur. As known, these mechanisms depend on factors such as the type of masonry and its quality, the flexibility of horizontal diaphragms and the effectiveness of structural connections (wall-to-wall, wall-to-floor and wall-to-roof), whose knowledge drives both the modeling assumptions and the choice of analysis methods. Past interventions and existing damage should be taken into account as well. The seismic capacity of URM structures is usually assessed through nonlinear analysis, as stated above due to the intrinsic inelastic behavior of masonry (limited capacity in tension and nonlinear response even for low or moderate stress levels) [6]. Both nonlinear static and dynamic analysis procedures can be applied, leading to large variability of results because of different modeling approaches, representations of the seismic action and calculation of its effects. Moreover, these procedures are strictly user-dependent, even with regard to ways of interpreting results and to requirements to be met, e.g. [7].

The modeling approaches for URM structures can be established at different scales depending on masonry quality, potential failure mechanisms and type of analysis [6]. Micro and meso models have been mostly used for analysis at element scale, especially for research purposes. These can be based on the finite element (FE) method or on the discrete element method [8] which is mostly suitable for regular masonry fabric [9]. Contrarily, macro modeling strategies based on application of the FE method (with plasticity or damage constitutive laws, see [10;11] respectively) or equivalent frame element and discrete methods (see [12–16]) are commonly used for seismic assessment at building scale. These strategies require less input data and lower computational effort, in particular at the analysis stage, but user expertise is still needed to obtain reliable results. Moreover, the application of any of these models in practice presents issues related to the representation of the geometry and structural details, the discretization of elements and the modeling of their mechanical behavior, as well as the definition of material properties, which are not significantly addressed in design codes, e.g. [17–20].

However, for any possible approach, the attainment of an adequate knowledge level is highly stressed in available codes for seismic safety assessment of existing buildings, especially URM ones. It can be erroneously assumed that for code-based designed modern buildings, the main epistemic uncertainties are only related to modeling the actions and their effects (material variability is somehow limited by quality systems during construction), while for existing buildings these uncertainties mostly refer to structural modeling. Indeed, this is true only to some extent because there are specific issues in the structural modeling of URM modern buildings which are still not addressed by standard codes resulting in the same uncertainties of existing structures,

e.g. the flange effect of orthogonal walls; see [21]. Epistemic uncertainties are also involved in the application of algorithms for generating the numerical models and in the arbitrary use of the software packages. For more advanced simulation approaches, the number of input parameters is normally higher and so the uncertainties are larger. In addition, despite the fact that these advanced numerical models are usually calibrated by inverse fitting against experimental data, e.g. from ambient modal identification, the corresponding results may be inaccurate as well. Indeed this calibration is based on the dynamic properties of a structure in its elastic range, but numerical predictions are usually made at ultimate state so the modification of those properties with increasing damage generates additional uncertainties [22].

This paper presents the results of the seismic assessment of two benchmark URM buildings obtained from a blind prediction test carried out by teams from different universities: École Polytechnique Fédérale de Lausanne - EPFL; Middle East Technical University - METU; University of Catania; University G. D'Annunzio of Chieti-Pescara; Delft University of Technology; University of Genova; University of Napoli Federico II; University of Pavia; and Yeditepe and Bogazici Universities. The exercise was made within the context of the *Special Session "Seismic modeling of masonry buildings: present knowledge and open challenges for research and practice"* during the 16th European Conference of Earthquake Engineering in Thessaloniki, Greece [23].

The case studies were two building configurations with different characteristics at material, structural element and global scales. The provided data are aimed at replicating the knowledge level in engineering practice for existing URM structures. The seismic capacity of the two building configurations was requested in terms of minimum values of PGA compatible with the attainment of the limit states of NC and DL, namely PGA_{NC} and PGA_{DL}, as well as the associated failure mechanisms. The participating teams were able to freely define the limit states to obtain the PGA values, to adopt code procedures applicable in their countries or to use more refined methods. A brief description of the adopted modeling strategies and methods of analysis was asked in addition to the indication of the design codes taken as reference. The aim of the exercise was to compare the adopted modeling strategies, the assumptions made about geometrical, structural and mechanical characteristics, the applied methods of analysis in the blind prediction test, as well as to evaluate the PGA dispersion resulting from all these factors influencing the seismic safety assessment. Despite the wide range of strategies used by the participant teams which reflects the few restrictions given in the instructions, not all the possible approaches for analyzing URM buildings are covered in the comparison made. Even if the set of analyzed tools and methods is not exhaustive, they reflect what is nowadays available to professionals and researchers at international level. This paper aims at providing an overview of the scatter observed in the blind prediction test, and at further addressing the open issues in seismic assessment procedures. The differences between the blind predictions made by the several teams are also given, but the estimation of weights of the adopted assumptions on these differences was not addressed, because it was out of the scope of the exercise.

2. Brief overview on other benchmarking studies available in literature

Since the early methods in the 1970s for the seismic assessment of URM buildings, increasingly complex approaches have been proposed. These are being incorporated in design codes and professional software. The benchmarking of practitioner-oriented software is an important task, either with regard to the identification of pros and cons for their application or with regard to the implementation of different numerical formulations.

Several studies [24–28], even when reducing the possible sources of dispersion, have demonstrated an excessively large difference between software predictions due to the arbitrariness in the modeling and analysis phases, as well as because of the adopted material models. In these
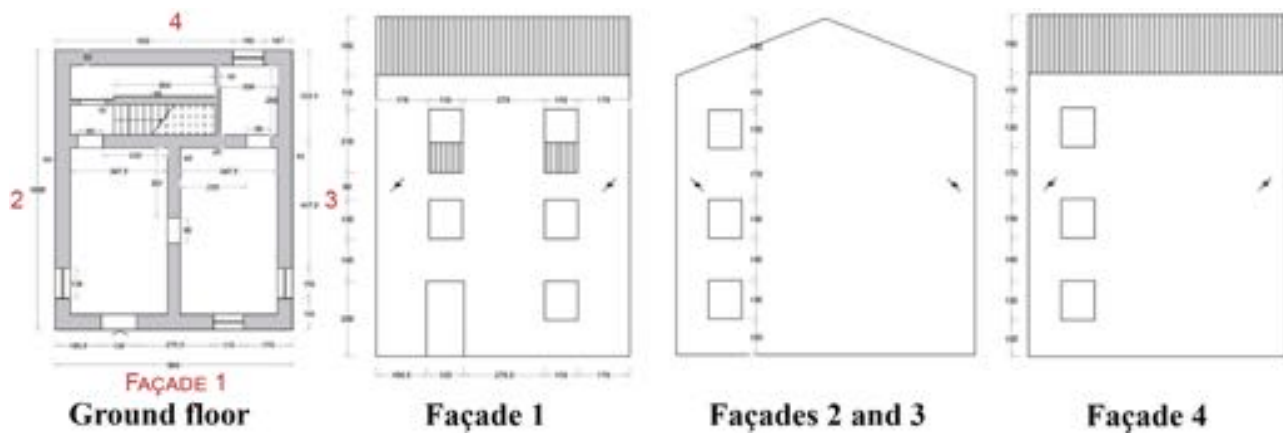
Fig. 1. Plan views of the case study buildings and the corresponding façades (wall thickness refers to Case A).

works, different numerical approaches were adopted resorting to general purpose and masonry-specific software, as well as to the implementation of a specific nonlinear algorithm in a MATLAB tool [29]. In the case of general purpose software, CDSWin-OpenSEES [30], MIDAS Gen [31], SAP2000 [32], DIANA FEA [33], and ANSYS [34] were used. In the case of masonry-specific software, 3Muri [12,35], Aedes.PCM [36], ANDILWall [37] and 3DMacro [13,38] were used. In a few cases, the predictions were validated against the results of the corresponding experimental tests, namely the ones carried out at the Portuguese Laboratory of Civil Engineering (LNEC) [39], at CNR-ENEA within the TREMA Project [40], and at Georgia Tech [41]. These were respectively considered as benchmark results by Aşıkoğlu et al. [24], by Betti et al. [26], and by Marques and Lourenço [27]. The load bearing walls of the structure tested at University of Pavia [42] were assumed as reference in Cattari et al. [25] for the external walls of an idealized building, varying its opening layout and structural details for the additional configurations.

The referred benchmarking studies were in general performed with reference to isolated two-story buildings with rigid or flexible horizontal diaphragms, particularly the prototypes in [39–42]. Masonry walls were considered to be made, according to the benchmark tests, of hollow concrete blocks in [24,28], irregular calcareous tuff stones in [26], and clay bricks in [25,27]. In each study, the modeling assumptions were defined by the authors as similar as possible for the different numerical approaches and computer codes, particularly in terms of geometrical discretization, to limit the variation of results and address their causes. The seismic capacity predictions, based on a simplified macro model by Galano and Selleri [29] in [26] and on a force-based method (proposed as an extension of RAN method by Augenti [43]) in [27], were cross-validated against the results from more complex approaches. The estimations were compared in terms of damage patterns, failure mechanisms and capacity curves for each URM structure.

The predictions from different structural component models by Marques and Lourenço [27,28] were consistent in terms of global collapse mechanisms, although some differences in the damage patterns and capacity curves were obtained. The capacity curves in [27] denote a different estimation of initial stiffness and base shear capacity (variation around 40%), but comparable values of yielding and ultimate displacement were predicted. In Betti et al. [26], the damage distributions, collapse mechanisms and capacity curves from a FE model were comparable to those from the experimental campaign at CNR-ENEA [40]. Contrarily, when adopting the macro element by Galano and Selleri [29], limitations were observed in capturing the evolution of damage and stiffness degradation of the tested prototype, thus the failure mode was not accurately predicted due to the simplified assumption of rigid diaphragms and spandrels. In Cattari et al. [25], the same structure was analyzed using different commercial software packages

thanks to the collaboration of several research teams, and by adopting, when possible, the same modeling assumptions in order to reduce the scatter of results. These results highlighted a difference in terms of base shear capacity around 30% for a structural configuration with weak spandrels and strong piers, and around 10% for shear type models (rigid horizontal diaphragms and spandrels with infinite stiffness and strength). The comparison in Aşıkoğlu et al. [24] demonstrated again the large variability of results with respect to base shear capacity and ultimate displacement. The numerical damage predictions were in reasonable agreement with the simulated experimental damage patterns, despite the first predictions were obtained from pushover analysis and the second ones from bidirectional dynamic tests. Moreover, the adopted spring-based discrete macro model by Caliò et al. [13] showed a dependency from the meshing of walls, in presence of a softening behavior, which increased the difference in predictions from the reference FE model.

In the present paper, after briefly describing the benchmark structures, a detailed overview of the results from the blind prediction test in [23] is presented. This overview highlights the numerical approaches and main assumptions made by each participant team. Again, a comparison between damage patterns, failure mechanisms associated to the minimum PGA_{NC} and PGA_{DL}, and capacity curves is made. Specifically, the seismic capacity is compared adopting as reference the PGA value representing the average of the minimum PGAs predicted for each limit state by the several teams. Moreover, the interpretation of in-plane (IP) and out-of-plane (OOP) failure modes predicted by each model is also given to provide a qualitative reliability measure of the modeling strategies and methods of analysis. Despite the fact that experimental testing of a building model would allow a more effective conclusion on the reliability of the numerical predictions, one can assume that the set of different approaches provides a range of predictions which define lower and upper bounds of the true response.

3. Description of the case studies proposed for the blind prediction

The benchmark URM buildings for the blind prediction test are briefly presented next, in terms of geometrical and structural configurations, as well as of masonry mechanical properties. Complementary input data are presented in the original document made available to the participants in the special session, which is included as supplementary material to make possible to other researchers to reproduce the same exercise.

The case studies are three-story buildings corresponding to two structural configurations with different types of masonry walls and of horizontal diaphragms:
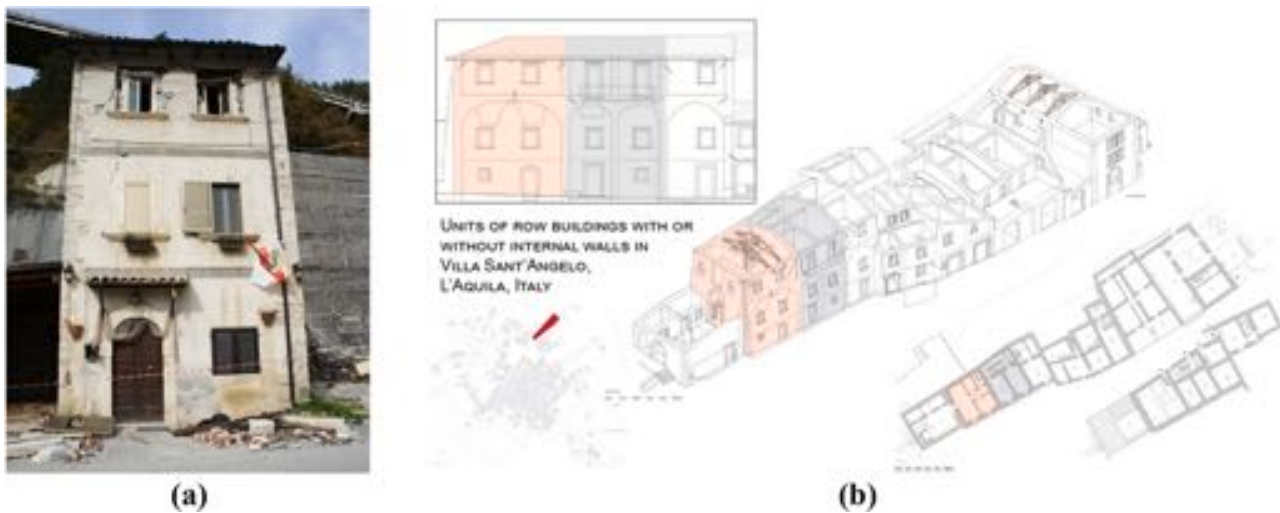
Fig. 2. Isolated building damaged by Amatrice-Norcia 2016/2017 earthquake in (a) and representative units in a building block of Villa Sant'Angelo (L'Aquila, Italy) in (b) [44].

Fig. 3. Typical OOP failure mechanisms in the 2009 L'Aquila earthquake with collapses of (a) gables and (b) main façades. Photo courtesy of Simone Del Grosso.

Case A) stone masonry and flexible diaphragms, comparable to a traditional non-engineered building;

Case B) brick masonry and rigid diaphragms, comparable to a modern code-based structure.

The geometrical and typological data, as well as the material mechanical properties, were defined to emphasize the main issues leading to arbitrariness in the seismic vulnerability assessment of existing URM constructions, such as:

  i. the prediction of potential failure mechanisms, either IP, OOP or their combination (IP + OOP), which may influence the choice of analysis method at local and global levels;
 ii. the modeling of structural elements such as piers, spandrels, stairs and diaphragms, as well as their connections and interactions;
iii. the assumptions on material properties;
 iv. the distribution of gravity loads;
  v. the representation of the seismic action;
 vi. the definition of criteria for limit states attainment and for the interpretation of results.

The geometrical layout of the buildings is rectangular in plan with

dimensions of 8.5 m × 10.0 m, and with 11.3 m in elevation (Fig. 1). For the sake of simplicity, the longitudinal direction refers to the shorter dimension in plan corresponding to Façade 1, while the transversal direction refers to the larger dimension in plan corresponding to Façade 2. External walls have regular openings vertically aligned with a maximum percentage of voids in Façade 1 (15.1%), a minimum percentage of voids in Façades 2 and 3 (4.2%), and a low percentage of voids (5.4%) in Façade 4 (Fig. 1). The inter-story height varies from 3 m at the ground and 1st floors, up to 3.35 m at the 2nd floor. A section view of the buildings is presented in the supplementary material.

The idealized geometrical layout is representative of existing URM building units in historical centers of Mediterranean and Central European countries, based on typological studies [44]. Although the building plan is regular in elevation, it presents some irregularities with respect to mass and stiffness distributions. External walls have regular but not symmetric openings to highlight the role of wall discretization in existing structures, e.g. Fig. 2a. Despite considering an isolated building, the architectural layout can also be representative of units in semi-detached buildings or aggregates in historical centers (Fig. 2b), once the case study buildings present a main front (Façade 1), stairs at the back, and a few openings in the remaining façades. This last characteristic stresses the frame-like assumption, thus allowing to discuss the range of applicability of equivalent frame based models for regular and

irregular URM walls, e.g. [45].

The representativeness of the case studies relates also to the typical failure mechanisms, especially OOP, which may occur during seismic events in both isolated and aggregated buildings. The collapse of gables and main façades is likely to happen due to ineffectiveness of structural connections, pounding of ridge beams or lateral thrusts from inclined roofs, as demonstrated in the post-earthquake scenario of the 2009 L'Aquila earthquake (Fig. 3a–b). Moreover, the two studied structures present floor types usually observed in existing buildings, e.g. [44], and their structural details rise additional issues related to their equivalent or explicit modeling, and related to the distribution of dead loads.

Regarding the masonry arrangement, the following types are considered in correspondence with the two structural configurations:

Case A) double-leaf walls consisting of cut stones arranged regularly and bonded with lime mortar, presenting through stones in the wall thickness;
Case B) English bond walls made with solid clay bricks and lime mortar.

The geometrical layout of Cases A and B is the same, except for the thickness of masonry walls which, in any case, decreases in elevation, with the exception of the internal walls (0.45 m for Case A and 0.25 m for Case B). For Case A, the thickness of the façade walls decreases from 0.55 m at the ground and 1st floors to 0.45 m at the 2nd floor, while in Case B from 0.38 m to 0.25 m. Details are given in the supplementary material to the paper.

The masonry spandrels include wooden lintels for Case A, and reinforced concrete (RC) beams for Case B. Moreover, in Case A, tie rods are applied at the 2nd floor, while in Case B the presence of RC slabs suggests an implicit connection to the walls through RC ring beams. This information has implications concerning the assumption of modeling the spandrels as coupling beams [17] and, consequently, in considering their IP failure mechanisms. For more information about cross-section dimensions and structural details, see the supplementary material to the paper.

The horizontal diaphragms have different IP stiffness (corresponding to flexible diaphragms with timber joists and single straight timber planks for Case A, and to rigid diaphragms with a RC slab for Case B) and deadweight (1.0 kN/m² for A and 3.5 kN/m² for B). Effective wall-to-floor connections and the same floor directions are assumed in both Cases A and B. One-way spanning floors are supported by all the internal and external walls, except Façade 1. Although the floor mass contribution is very limited in masonry buildings when compared to the mass of the walls, especially for configurations as Case A, an unloaded wall is likely to be more vulnerable to OOP mechanisms. A live load of 2.0 kN/m² is applied on each floor resulting from the residential use of the building (the quasi-permanent value of the live load is 0.6 kN/m²).

The roofing system is a double slope type consisting of a timber structure with rafters supported by joists (dimensions and details in the supplementary material). These joists are parallel to Façade 1 and rest on a beam (sill plate) above the internal longitudinal wall and on the two side Façades 2 and 3 (ending with a gable). The roofing system has an assumed dead load of 1.25 kN/m². The upper walls of Façades 1 and 4, as well as the gables of Façades 2 and 3 are potentially vulnerable to OOP failures, i.e. overturning, since they have limited vertical load.

Stairs are defined accordingly to the floor type: timber staircase and RC staircase with dead loads of 1.5 kN/m² and 3.5 kN/m², respectively for Cases A and B. The live load on the stairs is 4.0 kN/m² for both Cases (the quasi-permanent value of the live load is 1.2 kN/m²). The seismic response depends also on potential interactions with other structures and soil-foundations, but, in this case, they are both neglected, considering the buildings as isolated structures, with no basement and fixed at the base.

The mechanical properties for both masonry types are presented in Table 1. Input data are representative of those obtained from in situ tests and they are consistent with the mechanical properties given as reference in building codes, namely the Italian ones [18,46]. The provided values are mostly within the range prescribed in [46], corresponding to "cut stones with good texture" for Case A and "solid brick masonry with lime mortar" for Case B. No mechanical properties were provided for timber elements, concrete, steel reinforcement and tie rods, in order to reproduce a limited knowledge level for materials, resulting in additional requirements for assumptions and experience of the professional involved.

4. Modeling strategies and assumptions made by participant teams

As introduced in Section 1, the available modeling strategies for existing URM buildings vary in describing the structural behavior, from different scales in material constitutive models to macro element scale, as well as in terms of type of discretization for representing elements and damage. The decision on their use is usually supported by the characteristics of the building, particularly the connections between structural elements and the masonry quality, and so on the potential failure modes (IP, OOP, and IP + OOP). Ideally, this will determine the scale of analysis to perform (global and/or local). Moreover, this choice is influenced, in engineering practice, by the importance of the structure, the feasibility of the approach with respect to the available data and computational burden, as well as the required results, the budget available for the study, and the user expertise.

The seismic response of the two building configurations was simulated by the participating teams using both complex and simplified numerical models, for which a general overview is reported in this section focusing on the main hypotheses and assumptions, which are likely to influence the results. Open issues in the modeling of existing URM buildings are also addressed, even though within the range of computations performed by the participating teams. The modeling strategies adopted by the teams in the blind prediction test are grouped in the following relevant classes, based on the classification by Lagomarsino and Cattari [1]:

- Discrete Interface Models (DIM) for discrete schematization at material scale;
- Continuous Constitutive Law Models (CCLM) for continuous discretization at material level;
- Macro-Block Models (MBM) for discrete schematization at structural element scale;
- Structural Element Models (SEM) for continuous discretization at structural element level.

Table 1
Mechanical properties of masonry for building Cases A and B.

Case	E [MPa]	G [MPa]	w [kN/m³]	f_m [MPa]	τ_0 [MPa]	f_{bm} [MPa]	μ	f_{mt} [MPa]	f_{v0} [MPa]
A	1,750	550	21	3.2	0.065	–	–	–	–
B	1,500	500	18	7.5	–	14	0.6	0.12	0.2

E: elastic modulus, G: shear modulus, w: specific weight, f_m: masonry compressive strength, τ_0: masonry initial shear strength, f_{bm}: brick compressive strength, μ: mortar joint friction coefficient, f_{mt}: mortar joint tensile strength, f_{v0}: mortar joint initial shear strength. E and G refer to uncracked condition. All values are deterministic and representative of the mean value.

The different software packages used to simulate the seismic behavior of the building configurations are illustrated in Fig. 4, namely: 3DEC [47] whose formulation is based on the discrete element method for discontinuous materials; ELS – Extreme Loading for Structures [48], which is based on the applied element method for masonry structures; LUSAS [49], DIANA FEA [33], SAP2000 [32] and MIDAS Gen [31], which are multi-purpose computer codes based on the FE method; Aedes.PCM [36], ANDILWall [50] (currently PRO_SAM), 3Muri [35] and 3DMacro [38], whose application is masonry oriented and in which the structures are represented mostly according to the equivalent frame method or similar idealizations; OpenSEES [30], which is an open-source computational platform for research in performance-based earthquake engineering.

The identification of teams according to the above classification, together with the considered failure mode (IP, OOP, IP + OOP), is made in Fig. 5a-b, with RG-#, where # indicates the number of the participating team. An additional number follows the RG tag if the team considers more than one numerical model, e.g. RG-#_#. The modeling strategies were diverse for both Cases A and B, even though some teams (3 out of 9) only modeled Case B. Indeed, the characteristics of a code-based existing building make the modeling assumptions more straightforward than those for Case A. SEM based approaches were adopted by most teams (8 out of 9) in combination with DIM (RG-8_2 for Case A) or MBM (RG-9_2 for Case A and RG-8_3 for Case B) to check local OOP mechanisms, or as a simplified strategy complementary to a CCLM based approach (RG-1_2).

In a few cases (2 out of 9) the participants only considered IP mechanisms, thus the resulting predictions may be unsafe, if OOP collapses occur. Approaches based on combined failure modes (IP + OOP) were used by 4 out of 9 teams using different strategies such as DIM (RG-2_1), CCLM (RG-1_2, RG-5) and SEM (RG-1_1, RG-4). The selection of such approaches potentially increases the dispersion of results, not only because of different modeling assumptions, but also due to the arbitrariness in defining the attainment of limit states for combined failures.

RG-2 team used also an elastic FE model (CCLM) to validate the modal parameters of DIM (RG-2_1), and a hybrid strategy between CCLM and SEM for a 2D analysis of Façade 1 (RG-2_3) for Case B. A reverse approach was applied by RG-6 team for Cases A and B, which consisted on using an elastic FE model only to verify the a priori hypotheses about the most critical structural elements with respect to IP and OOP mechanisms.

The main assumptions in terms of geometry, material properties and load distribution for each modeling strategy are briefly reported and discussed in the following subsections.

4.1. Discrete interface models (DIM)

The approach is characterized by modeling the material as an assemblage of distinct elements interacting along their boundaries. This approach is particularly suitable for blocky masonry, but its application can be extended to any kind of masonry by performing homogenization procedures resulting in simplified discretizations that may affect the response [9].

Only one team (RG-2) modeled the whole building (Case B) using this strategy based on the discrete element method, but a similar approach based on the applied element method by Meguro and Tagel-Din [51] was also adopted by RG-8 team to assess the OOP vulnerability of Façade 1 in Case A. This approach has been tested for other URM case studies as described in [52]. In both cases, masonry units were considered as rigid elements and deformations were lumped at interfaces that have zero thickness. In the model of Case B by RG-2 team (RG-2_1), this last assumption resulted in some differences of geometrical dimensions for the case study. Regarding the horizontal diaphragms, RC slabs were modeled as rigid and the members of timber roof were also considered as rigid elements. Inclined rigid blocks were used for the stairs as well. The numerical model of Façade 1 in Case A by RG-8 team (RG-8_2) matches the given geometry, although the masonry arrangement was simplified by adopting regular blocks. Tie rods were modeled at the 2nd floor, since their contribution influences the OOP response.
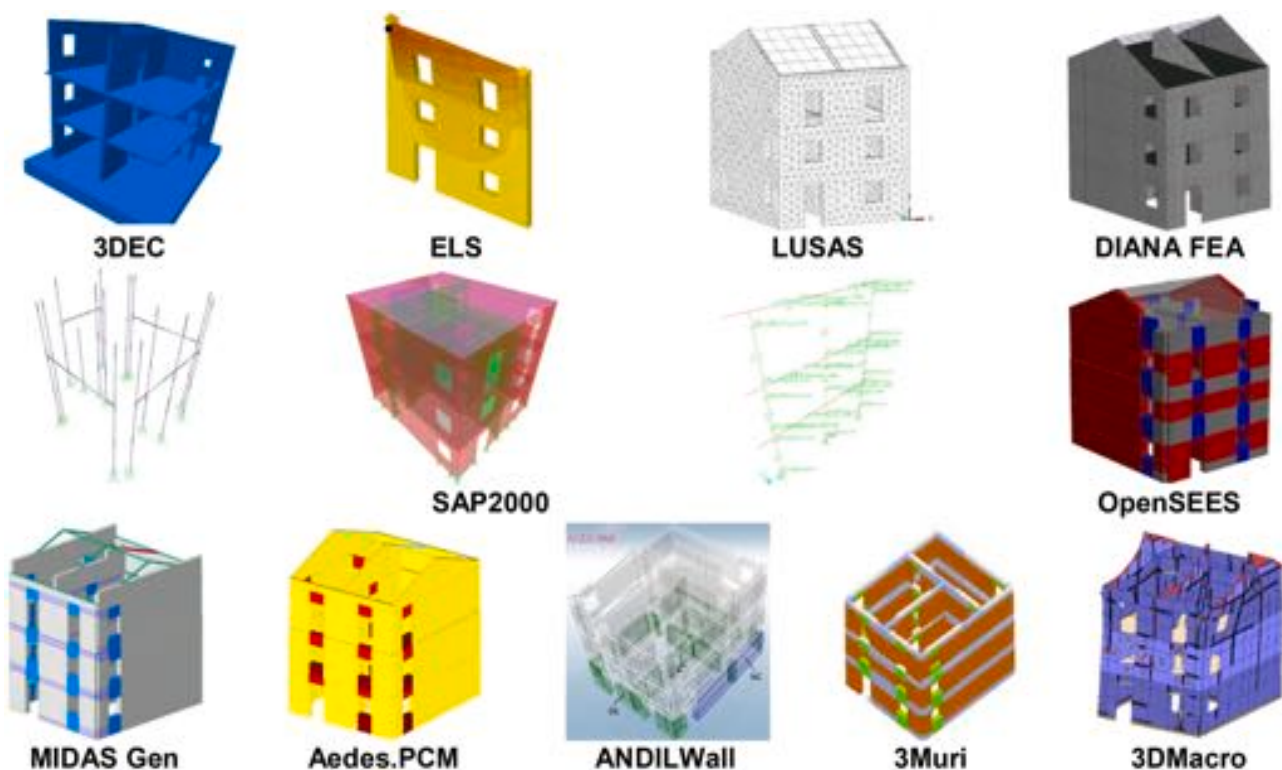

Fig. 4. Software packages adopted by participating teams.
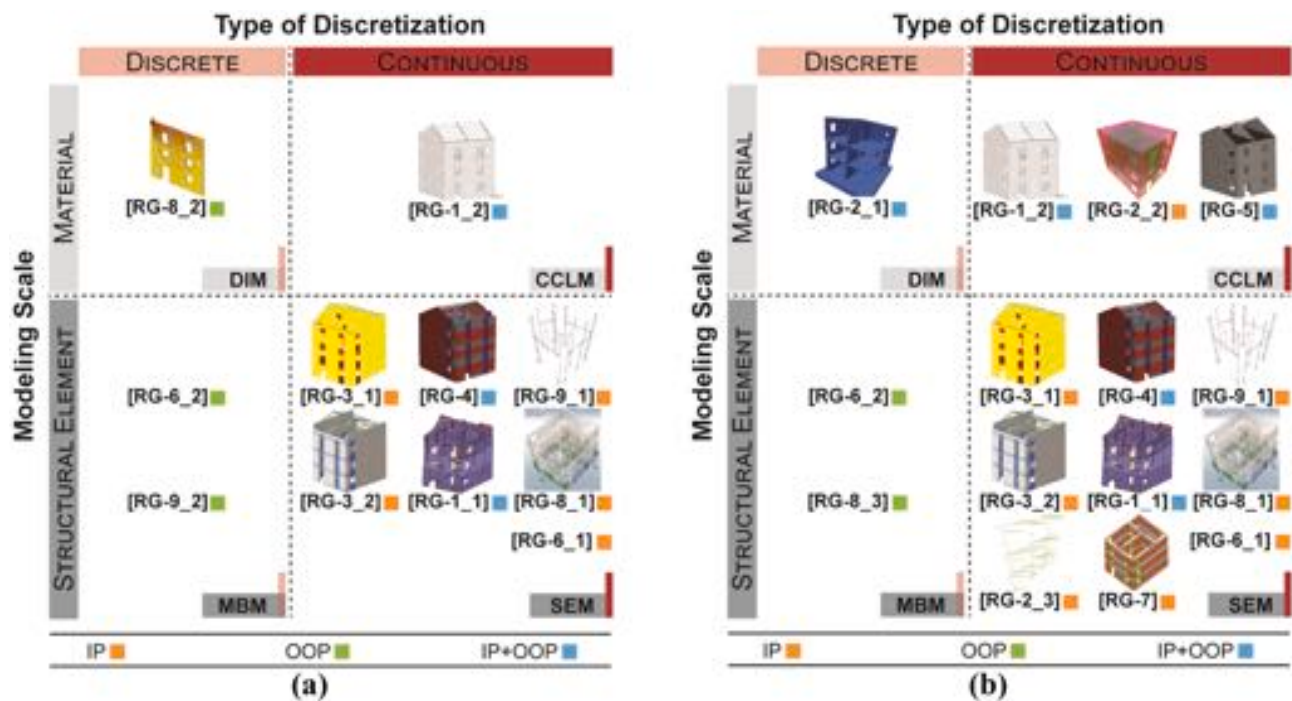
Fig. 5. Modeling strategies adopted by participating teams with related failure mode: (a) Case A and (b) Case B.

The nonlinear behavior of springs connecting the rigid units and representing the mortar joints was considered by RG-2 team according to a Coulomb slip model by setting the normal and shear stiffness, cohesion, tensile strength and friction angle (RG-2_1). In turn, RG-8 team considered a composite interface cap model with a Mohr-Coulomb criterion and a tension cut-off (RG-8_2). In this last case, the normal and shear stiffness values of the mortar joints were defined according to the homogenized elastic masonry properties.

4.2. Continuous constitutive law models (CCLM)

In FE based models, masonry is represented as a homogeneous material and its nonlinear behavior is described by means of specific constitutive laws whose properties may require additional assumptions, thus potentially increasing the dispersion of results. In this case, arbitrariness is also related to the choice of element type, meshing algorithm, element size and mesh quality parameters (many of these being user-dependent). There is some consensus that element size should be defined according to preliminary numerical sensitivity analysis, but

Table 2
Modeling assumption for approaches based on CCLM.

Approach	Case	Walls	Lintels	Floors	Roof	Connections			Stairs
						W-W	W-F	W-R	
RG-1_2	A and B	Nonlinear solid FE	–	Elastic shell FE	Reduced-stiffness elastic shell FE	*	⊣	⊣	Reduced-stiffness elastic shell FE
RG-2_2	B	Linear shell FE	Elastic beam FE	Elastic shell FE	Elastic shell FE	*	⊣	⊣	Elastic shell FE
RG-5	B	Nonlinear shell FE	Elastic beam FE	Elastic shell FE	Explicit elastic beam FE	*	⊣	⊣	Elastic shell FE

The connections refer to W-W: Wall-to-Wall, W-F: Wall-to-Floor, W-R: Wall-to-Roof.
Type of connection W-W: * effective connection.
Type of connection W-F or W-R: ⊣ effective connection.

Table 3
Mechanical properties of materials assumed by RG-5 team.

Case	Masonry			Timber		Concrete	
	E_x	G_{fc}	G_{ft}	E	ν	E	ν
	[MPa]	[N/mm]	[N/mm]	[MPa]		[MPa]	
B	750	18.02	0.009	12,000	0.3	29,000	0.2

The values refer to E: elastic modulus, E_x: elastic modulus in direction parallel to bed joints, G_{fc}: compressive fracture energy, G_{ft}: tensile fracture energy, ν: Poisson's ratio.
The fracture energy values in compression and tension were calculated based on the following formulas Eqs. (1) and (2), given in [56]:

$$G_{fc} = 15 + 0.43 \cdot f_c - 0.0036 \cdot f_c^2 \tag{1}$$

$$G_{ft} = 0.025 \cdot (2 \cdot f_t)^{0.7} \tag{2}$$

there is less consensus on using linear vs. quadratic FEs, on using shells vs. volume FEs, or on the usage of through thickness integration in shell FEs, just to name a few.

For the approach with CCLM, the discretization of the buildings was made by RG-1 team using a combination of solid FEs for walls and shell FEs for diaphragms (RG-1_2), and by RG-5 and RG-2 teams adopting shell FEs for both walls and diaphragms (RG-5 and RG-2_2, respectively). However, RG-2 team performed the seismic assessment by considering a simplified 2D model of Façade 1 (RG-2_3), as previously mentioned.

The modeling assumptions in terms of FE discretization for approaches based on CCLM are listed in Table 2. The horizontal diaphragms were in general modeled using elastic shell FEs with equivalent properties assumed according to the structural details proposed for Cases A and B. An explicit modeling approach was considered by RG-5 team for the roof members and for the RC lintels by using elastic beams perfectly connected at their ends to side walls. Effective connections between structural elements were assumed by all teams, but stairs were not connected to side walls in the shell FE model by RG-5 team, resulting in a reduction of wall restraints due to the physical gap that influenced the OOP behavior.

Variability of the results is likely to be increased when defining the input data for masonry material models, such as the fracture energy in compression and tension for the engineering masonry model [53] in DIANA FEA software [33] by RG-5 team. Additional dispersion is likely to occur due to the definition of material properties for timber or RC, and also due to the homogenization process to determine the equivalent characteristics of horizontal diaphragms. RG-2 team assumed a C20/25 concrete class to define the equivalent properties of RC diaphragms, while RG-5 team considered just the stiffness properties for timber and RC materials according to classes C30 in [54] and C16/20 in [55], respectively (Table 3).

Arbitrariness is also related to the distribution of floor gravity loads to side walls. In particular, RG-5 team considered a small sharing of load from floors to the unloaded side walls. The load applied over strips of 1.0 m from the border was assigned to those longitudinal side walls, although floors are one-way spanning; see supplementary material. This assumption is discussed in more detail in the following subsection.

4.3. Structural element models (SEM)

SEM based approaches consider a macroscopic description of the behavior of each structural component according to homogenized material properties [1]. The application of these approaches is widespread in engineering practice, although the arbitrariness in its application is still large, as reported in [57].

Almost all teams (8 out of 9) adopted SEM, but their assumptions in terms of geometry of structural components, material properties and load distribution were very different, as demonstrated by the following subsections. However, most teams (4 out of 8) considered only IP failure modes according to the box-like behavior hypothesis, by assuming good masonry quality, sufficiently stiff diaphragms and effective wall-to-wall and wall-to-floor connections. Other modeling strategies were applied in combination with SEM to check OOP failure modes; see Subsections 4.1 and 4.4.

4.3.1. Discretization of structural components

This subsection addresses the geometrical and structural assumptions made by each team for modeling the walls, diaphragms and their connections. These assumptions are reported in brief in Table 4 and discussed to clarify their influence on the seismic assessment.

Since many SEM based approaches derive from the equivalent frame method, namely through discretizing masonry walls as an assemblage of deformable (piers and spandrels) and rigid (nodes) parts, the first source of dispersion is the definition of the effective height of piers. Teams RG-2 and RG-4 applied the Full Rigid Offset method in [20], while RG-9 team defined the piers using a modified approach of this last method, i.e. considering the deformable height as the one of the adjacent openings for confined piers and adding half height of the node for unconfined piers. The method by Dolce [58] was assumed by RG-3 and RG-8 teams, while RG-7 team used the criterion implemented in 3Muri software [12]. The discrete macro element approach by Caliò *et al.* [13] adopted by RG-1 team is hybrid between CCLM and SEM strategies because each structural component can be discretized either as one single panel or with several discrete elements simulating the combined IP and OOP behavior of masonry walls. This approach considers all the structural components as deformable and the wall discretization resulted from the openings layout. In global analysis with SEM, the OOP stiffness of masonry walls orthogonal to the seismic action is usually neglected [57],

Table 4
Modeling assumptions for approaches based on SEM.

Team	Case	Effective height of piers	Spandrels	Floors	Roof	Connections			Stairs
						W-W	W-F	W-R	
RG-1	A	–	Coupling beams	Finite stiffness elastic orthotropic shell FE	No diaphragms (RG-1_1) Zero-stiffness elastic shell FE (RG-1_2)	*	⊣	⊣	Completely flexible
	B			Rigid shell FE					Finite stiffness elastic shell FE
RG-2	B	Full Rigid Offset	Coupling beams	Finite stiffness	Finite stiffness	*	⊣	⊣	Finite stiffness
RG-3	A	Dolce's method	Coupling beams	Finite stiffness	Explicit modeling with elastic beams	*	⊣	⊣	Not modeled
	B			Rigid					
RG-4	A	Full Rigid Offset	Coupling beams	Finite stiffness orthotropic membrane	Finite stiffness orthotropic membrane	***	//	⊣	Finite stiffness orthotropic membraneRigid elastic shell FE
	B			Rigid elastic shell FE					
RG-7	B	3Muri's method	Coupling beams	Rigid orthotropic membrane	Finite stiffness orthotropic membrane	**	⊣	⊣	Rigid orthotropic membrane
RG-8	A	Dolce's method	Coupling beams	Finite stiffness	Finite stiffness	*, **	⊣	⊣	Finite stiffness
	B			Rigid with different classes of reinforcements		*			Rigid
RG-9	A	Modified Full Rigid Offset	Trusses	No diaphragms	No diaphragms	*	–	–	Not modeled
	B		Trusses	Rigid		*	⊣	–	

The connections refer to W-W: Wall-to-Wall, W-F: Wall-to-Floor, W-R: Wall-to-Roof.
Type of connections W-W: * partial connection, ** effective connection with L or T sections, *** connection by zero-length elements
Type of connections W-F or W-R: ⊣ effective connection, // connection by interfaces.

due to its small contribution. However, RG-8 team analyzed Case B either considering or neglecting this contribution to determine its influence on the global response.

Spandrels were considered as equivalent coupling beams [17] by most of teams for both configurations, although in Case A this assumption only applies to those at the 1st floor due to the presence of tie rods. However, this coupling behavior was neglected by RG-9 team, which modeled all spandrels for Case A and B as trusses just to couple the horizontal displacements between piers at floor level.

Regarding horizontal diaphragm modeling, a large variation was observed again, especially in Case A, due to the arbitrariness in their consideration, ranging from the lack of floors to finite stiffness diaphragms. RG-3 team considered diaphragms with limited IP stiffness, which were modeled using elastic shell FEs. Teams RG-1, RG-4 and RG-7 adopted orthotropic elastic membrane FEs, for which a reduced stiffness was estimated in the weak direction; see Table 4. The predicted response of the buildings is likely to be influenced by the different approaches, since floors play a fundamental role in distributing seismic forces to masonry walls. RC slabs in Case B were in general modeled using elastic shell FEs. RG-8 team performed numerical sensitivity analysis varying the class of steel reinforcements for the RC slabs (FeB22k and B450C according to [18]) to estimate their influence on the global response.

The vertical load distribution was in general based on the tributary area of each wall, thus resulting in point masses lumped at structural nodes of the walls. Some teams (RG-1, RG-2, RG-3, RG-4 and RG-7) strictly considered the floor spanning directions, while others (RG-8 and RG-9, as well as RG-5 for CCLM) shared a percentage of vertical loads to walls parallel to floor directions. This assumption is justified if the shared load corresponds to limited strips with dimensions comparable to the spacing of timber joists (0.5 m) for Case A, and of RC ribs between hollow blocks incorporated into the slab thickness for Case B. In addition to the floor aspect ratio and its structural details, the presence of concrete overlay in Case B, and the compatibility of displacements results in the same load migration.

For example, RG-9 team considered a small sharing to these walls calculated for strips of 0.5 m and 1.0 m for Cases A and B, respectively. RG-8 team studied the influence of the vertical load distribution on the global response with reference to two different load proportions for Case B, in the main and orthogonal directions, respectively: 80% and 20%, and 90% and 10%.

The dispersion related to modeling timber diaphragms is even higher for the roofing system. RG-3 team modeled explicitly the components of the roof (ridge beam and sill plates above side and internal walls in the supplementary material) as elastic beam elements in RG-3_2 model, while the remaining teams considered an equivalent diaphragm. In case of an equivalent diaphragm, the choices vary from zero-stiffness FE diaphragms (RG-1_2) to finite stiffness membrane elements (RG-2, RG-4, RG-7 and RG-8 teams); see Table 4. In the models by teams RG-9 and RG-1 (RG-1_1) there is no roof, consistently with the lack of floors.

Although the stairs have influence on the dynamic behavior of the structure, they were not always modeled (RG-3 and RG-9 teams), for simplification. The remaining teams represented them using the same approach adopted for the timber diaphragms.

The arbitrariness was further increased when considering different assumptions for wall connections. A numerical sensitivity analysis was performed by RG-8 team concerning this aspect for Case A, considering full connections with T/L shapes at the wall intersections and corners or partial connections with related piers presenting rectangular cross-sections coupled by means of rigid or finite stiffness beams at floor level. This last assumption results in a variation of the normal load and stiffness, but the wall resistance is still calculated based on the uncoupled section. A different approach was used by RG-4 team that connected orthogonal piers with zero-length elements considering a possible failure in tension; see Table 4.

Wall-to-floor connections were considered always effective, according to the information provided to participants, with the exception of

RG-4 team that modeled an interface with perfectly plastic frictional behavior and a maximum slip (0.2 m). The friction coefficient between mortar and timber was set to 0.4 for Case A, while the one between masonry and concrete was set to 0.7 for Case B.

4.3.2. In-plane response of structural components

SEM approaches were traditionally developed based on evidence of damage during seismic events. This is because their occurrence is assumed in particular sections of piers and spandrels [9]. In these sections, the structural behavior is modeled through nonlinear elements whose moment–rotation or force–drift relationships describe the lateral IP response of the component in terms of global stiffness, ultimate strength and either drift or rotation capacity. An overview of the assumptions on modeling this IP response is presented here.

The selection of specific elements with nonlinear relations depends on the potential failure mechanisms and the related ductile or brittle behavior as observed in experimental tests [59,60]. Based on the type of masonry, different IP failure mechanisms may be expected, such as flexural or horizontal sliding at the ends of each element, and diagonal cracking or sliding at its mid part. Flexural and diagonal cracks are likely to occur if the masonry pattern is irregular (Case A), while flexural, horizontal and diagonal stair-step cracks may occur for regular ones (Case B). These mechanisms were considered for piers and also for spandrels if modeled as coupling beams. The shear capacity of these elements is usually derived based on strength criteria aimed to correlate the material properties to the overall response of structural components [61,62].

Different relationships related to the identified mechanisms were considered, i.e. elastic–perfectly plastic (RG-3, RG-7, RG-8 and RG-9 teams), bilinear with softening (RG-2 team), elastic–plastic brittle with residual strength (RG-8 team) and multilinear (RG-2 team); see Fig. 6a-d. The dispersion further increases due to the different drift or rotation thresholds assumed by each team, highlighting again the large arbitrariness in practice; see Table 5. These threshold values were defined consistently with the reference design codes, [3,63], for RG-4 (Case B) and RG-3 teams, slightly modified from the same codes (RG-7, RG-8 and RG-9 teams), or taken from recommendations in the literature. RG-4 team assumed for Case A these thresholds based on a dataset of the drift capacity of stone masonry walls by Vanin et al. [64], while the strain ductility values recommended by Knox [65] were considered by RG-2 team for Case B. The scatter is further increased if the change of axial load (N) on piers is considered for their lateral resistance by coupling axial load with the bending moment (M), defining a N–M envelope for the plastic hinge (RG-2 and RG-9 teams for Case B). The change of N mainly occurs if piers are coupled by effective spandrels [17], otherwise a flexural plastic hinge can be adopted (RG-9 team for Case A).

Anyway, the behavior of piers and spandrels can also be modeled by using structural elements with both IP and OOP degrees of freedom. RG-4 team developed a macro element in OpenSEES software [30] as an assemblage of two blocks which are deformable in shear and can rock for IP and OOP over the three interfaces at the ends and mid-point [66]. The envelope of the cyclic response of this macro element (Fig. 7) can be assumed as elastic–perfectly plastic for flexure (Type 1, see Fig. 6a), and bilinear with softening for shear (Type 2, see Fig. 6b). Regarding the OOP flexure, the lateral resistance approaches the rigid body rocking solution since second-order effects are considered (Type 2, see Fig. 6b).

RG-1 team utilized the discrete macro element developed by Caliò et al. [13], which is incorporated in 3DMacro software [38]. In this case, masonry walls are discretized by means of quadrilateral elements with rigid edges connected among opposite corners by diagonal nonlinear springs. Each element interacts to the adjacent ones by means of zero-thickness interfaces with distributed nonlinear (flexural and shear) links along each side of the element. Orthogonal springs simulating the flexural behavior present an elastic–perfectly plastic relation (Fig. 6a) with a given rotation based on the maximum compressive and tensile
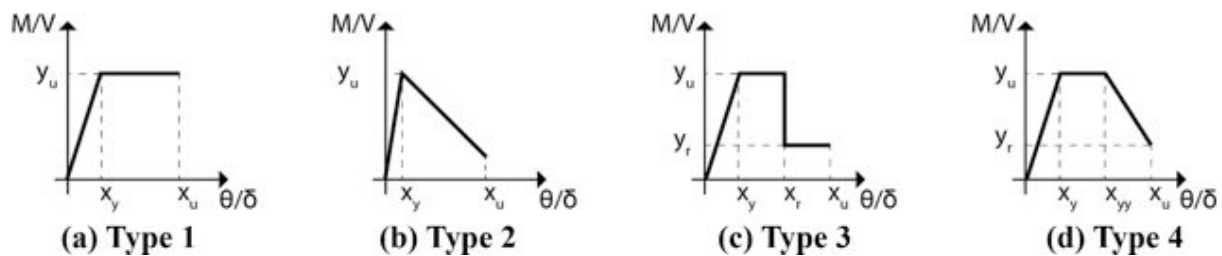
Fig. 6. Schematic moment–rotation or force–drift relations: (a) elastic–perfectly plastic, (b) bilinear with softening, (c) elastic–plastic brittle with residual strength and (d) multilinear.

strains [13]. Transversal springs modeling the sliding shear follow a rigid-plastic relationship governed by a Mohr-Coulomb yielding criterion. The response of the diagonal springs simulating the diagonal shear can be based either on the Turnšek and Čačovič [67] or Mohr-Coulomb strength criteria, and with the ultimate shear displacement directly related to a limiting drift defined in design codes, e.g. [3,63], or obtained from experimental tests, e.g. [62].

4.4. Macro-block models (MBM)

MBM approaches are usually applied to existing URM structures without box-like behavior, by considering an assemblage of rigid blocks for portions of the structure (usually walls or parts of walls) [9]. These blocks are defined based on evidence of damage to buildings during seismic events, which simulate the observed failure modes, e.g. [68]. This modeling approach considers the potential collapse mechanisms of macro blocks according to a limit analysis under the conditions by Heyman [69] originally proposed for the behavior of masonry arches (zero tensile strength, no sliding between blocks and infinite compressive strength), then extended to URM buildings.

Although this strategy could have been used to assess potential local mechanisms in Case A, namely overturning or vertical arching, especially for Façades 1 and 4, it was only applied by one team. These OOP mechanisms are strictly related to the structural characteristics of the buildings. Indeed, the double slope roofing system can result in lateral thrusts not resisted by side walls due to the lack of tying elements at the upper level of the building, in both Cases A and B. For Case B, these thrusts can be avoided by the presence of a RC tie beam, but no information was provided in this respect (thus, the assumption on the most probable behavior was to be determined by the research teams). Moreover, in Case A, the presence of tie rods at the 2nd floor can lead to potential vertical arching mechanisms of the lower part of Façade 1 or overturning mechanisms of its central wall, since it is unloaded and may not be sufficiently restrained by floors, even though effective connections wall-to-floor were stated in the data sheets; see Section 3. Similar vulnerabilities can be identified for Façade 4, in which the restraint of timber stairs is limited and the façade span is not reduced by any transversal internal wall.

The OOP vulnerability of the central wall of Façade 1 for Case A was assessed only by RG-9 team considering no restraint of tie rods and ineffective wall-to-floor and wall-to-wall connections. RG-8 team adopted MBM in Case B to assess the overturning mechanism of gables. This is consistent with the fact that existing URM buildings are highly vulnerable to this type of OOP mechanism as observed in post-earthquake scenarios, e.g. 2009 L'Aquila earthquake (see Fig. 3). The activation of the mentioned mechanism largely depends on the structural connection between the gable walls and timber struts that may cause the expulsion of the external leaf of the wall, or more severe damage.

5. Methods of analysis

The seismic vulnerability assessment can be performed by means of global or local analyses based on the initial assumptions about potential failure mechanisms. Global analysis ensures reliable results for structures with a prevailing IP behavior of walls, effective wall-to-wall, wall-to-floor and wall-to-roof connections, and sufficiently stiff diaphragms, while local analysis should be performed if existing structures do not evince these features. The scale of analysis can consider sequentially global and local effects, or vice-versa, once the structural elements most likely to be damaged are identified. Methods of analysis also vary in terms of description of structural behavior, from linear to nonlinear, and in terms of calculation of seismic effects by solving equilibrium equations statically or dynamically, meaning different representations of seismic actions.

An overview of the analysis methods used by the participating teams is presented in Fig. 8. Again, after the identification of each team and modeling strategy, an additional letter follows this tag if the team considered more than one analysis, e.g. RG-2_2a. In most cases, nonlinear static (pushover) and dynamic (time-history) analyses (NLSA and NLDA respectively) were performed since linear analysis has limited application for masonry [5]. However, RG-6 team performed linear static analysis (LSA) in combination with linear kinematic limit analysis (LKLA) for the analysis of OOP mechanisms for Cases A and B.

RG-8 team used LKLA and nonlinear kinematic limit analysis (NLKLA) to study the local OOP behavior for Case B. For Case A, LKLA was also applied by RG-9 to assess the OOP vulnerability of Façade 1. Such limit analysis methods can assess only NC conditions since they are based on the upper bound theorem of plasticity. RG-2 team performed eigenvalue analysis (LDA) of a shell FE model (RG-2_2) to compare the resulting modal parameters with those from the DIM in 3DEC (RG-2_1) before performing NLDA. Moreover, LSA was carried out using a hybrid shell-frame model (RG-2_2) to calculate the axial load on the piers of Façade 1. Finally, NLSA and incremental NLDA were applied to an 2D equivalent frame-based model (RG-2_3) with lumped plasticity at element ends.

The main assumptions in terms of representation of the seismic action, definition of control points and additional input for nonlinear analyses, are briefly reported and discussed in the following, as well as the requirements to be met for the adopted criteria at both limit states of NC and DL.

5.1. Assumptions regarding nonlinear analysis procedures

The arbitrariness in the application of nonlinear analysis methods can be large, as well as in the choice of the appropriate engineering demand parameter to define the attainment of limit states. For pushover analysis, the global response of a building corresponds to the relation between base shear force and displacement at a control node selected by the user. The seismic forces are usually simulated by applying two load patterns: "modal" distribution, proportional to the fundamental mode shape of the building, and "uniform" distribution, proportional to mass. Other load patterns may be chosen, e.g. a triangular shape may be used as a simplification of the first mode proportional. The verification procedure consists of comparing demand against capacity, which are both referred to an equivalent SDOF system whose properties consider the
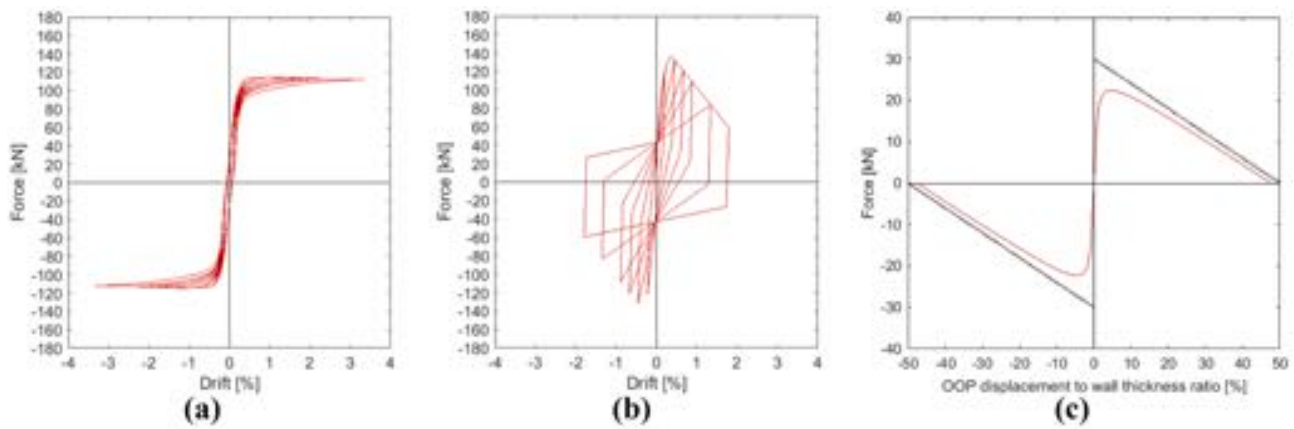
Fig. 7. Macro element cyclic response in (a) flexure, (b) shear and (b) OOP rocking, by RG-4 team.

nonlinear behavior of masonry. Since the dynamic behavior of a building is implicitly considered in NLDA, the arbitrariness relates to the representation of seismic action and to the interpretation of results in the post-processing phase.

As expected, the variability for Case A was larger than the one for Case B, because in the first configuration, the assumptions resulting from the box-like behavior do not apply. The provided data limit the arbitrariness, specifying the seismic action according to Eurocode 8 Part 1 [17], but still the range of variation of its representation among the teams was quite large. Type 1 elastic response spectrum was assumed to describe the seismic action, considering soil class B and the corresponding parameters as given in the supplementary material.

Therefore, the seismic action for NLDA was represented with a sufficiently large set (3 ÷ 7) of recorded or synthetic accelerograms by RG-4 and RG-5 teams, and by RG-2 and RG-8 teams, respectively. The accelerograms were scaled or generated to match the assumed shape of the response spectrum (Fig. 9a-b). NLDA were performed combining the effects of horizontal components of the seismic action as recommended in [17], except in those by RG-8 and RG-2 teams. For RG-8 team, the seismic action was only applied in the transversal direction to investigate the OOP behavior of Façade 1 for Case A (RG-8_2), while for RG-2

team, the action was only considered in the longitudinal direction of the building for Case B (RG-2_1) and parallel to Façade 1 to estimate its IP response (RG-2_3b); see Table 6. However, no research team considered the combined effects of horizontal components of the ground motion with the vertical one. Indeed, there are not many studies on the topic in literature, and especially for NLSA it is still not clear how to combine the seismic-induced vertical and horizontal loads. Concerning the dynamic response, the simultaneous application of horizontal components and the vertical one may result in instantaneous amplifications or reductions of the building seismic response. However, the few studies available in literature are still inconclusive whether the results obtained by neglecting the vertical component are conservative or unsafe (e.g. see [70,71]). Also the Codes are not unanimous about this effect: the New Zealand guidelines for seismic assessment of buildings [19] state that the vertical acceleration may be neglected when assessing the stability of masonry walls, while other Codes (e.g. Eurocode 8 Part 1 [17] or the Italian Building Code [18]) indicate specific situations in which it should be considered although they are valid for all the structural typologies and not specifically masonry oriented (e.g. in presence of large spans or horizontal pre-stressed components, just to name a few).

In NLDA, the choice of a damping model and the related parameters

Table 5
Modeling assumptions for the IP response of piers and spandrels in approaches based on SEM.

Team	Approach	Pier		Spandrel	
		Failure mode	Description	Failure mode	Description
RG-1	HY	Flexural	Type 1 with max drift of 0.6%	Flexural	Type 1 with max drift of 0.6%
		Diagonal cracking/ sliding for A and B	Rigid–plastic relation (Mohr-Coulomb criterion)	Diagonal cracking/ sliding for A and B	Rigid-plastic relation (Mohr-Coulomb criterion)
RG-2	LP	Flexural	N–M - Type 4 with max rotation of 2%	Flexural	M - Type 1 with max rotation of 1.5%
		Diagonal sliding	L - Type 2 with softening at 0.008% drift and max drift of 1%	Diagonal sliding	L - Type 2 with plastic branch from 0.009% to 0.8% drift and max drift of 1.6%
RG-3	LP	Flexural	Type 1 with max drift of 0.8%	Flexural	Type 1 with max drift of 0.8%
		Diagonal cracking/ sliding for A and B	Type 1 with max drift of 0.4%	Diagonal cracking/ sliding for A and B	Type 1 with max drift of 0.8%
RG-4	–	Flexural	Max drift is 1% (A) and 0.8% (B)	Flexural	No drift limits
		Diagonal cracking/ sliding for A and B	Max drift is 0.7% (A) and 0.4% (B)	Diagonal cracking/ sliding for A and B	No drift limits
RG-7	LP	Flexural	Type 1 with max drift of 1%	Flexural	Type 1 with max drift of 1%
		Diagonal sliding	Type 1 with max drift of 0.5% (Mohr-Coulomb criterion)	Diagonal sliding	Type 1 with max drift of 0.5% (Mohr-Coulomb criterion)
RG-8	LP	Flexural	Type 1 with max chord rotation of 1%	Flexural	Type 1 with max chord rotation at 2%
		Diagonal cracking/ sliding for A and B	Type 1 with max chord rotation of 0.5%	Diagonal cracking/ sliding for A and B	Type 3 with a 40% strength degradation at 0.5% chord rotation and a maximum chord rotation of 1.5%
RG-9	LP	Flexural	M (A), N–M (B) - Type 1 with max drift of 0.6%	Flexural	M - Type 1 with max drift of 0.6%
		Diagonal cracking/ sliding for A and B	M - Type 1 with max drift of 0.4%	Diagonal cracking/ sliding for A and B	M - Type 1 with max drift of 0.4%

The acronyms stand for A: stone masonry structure, B: brick masonry structure.
LP: Lumped Plasticity, HY: hybrid discrete macro model.
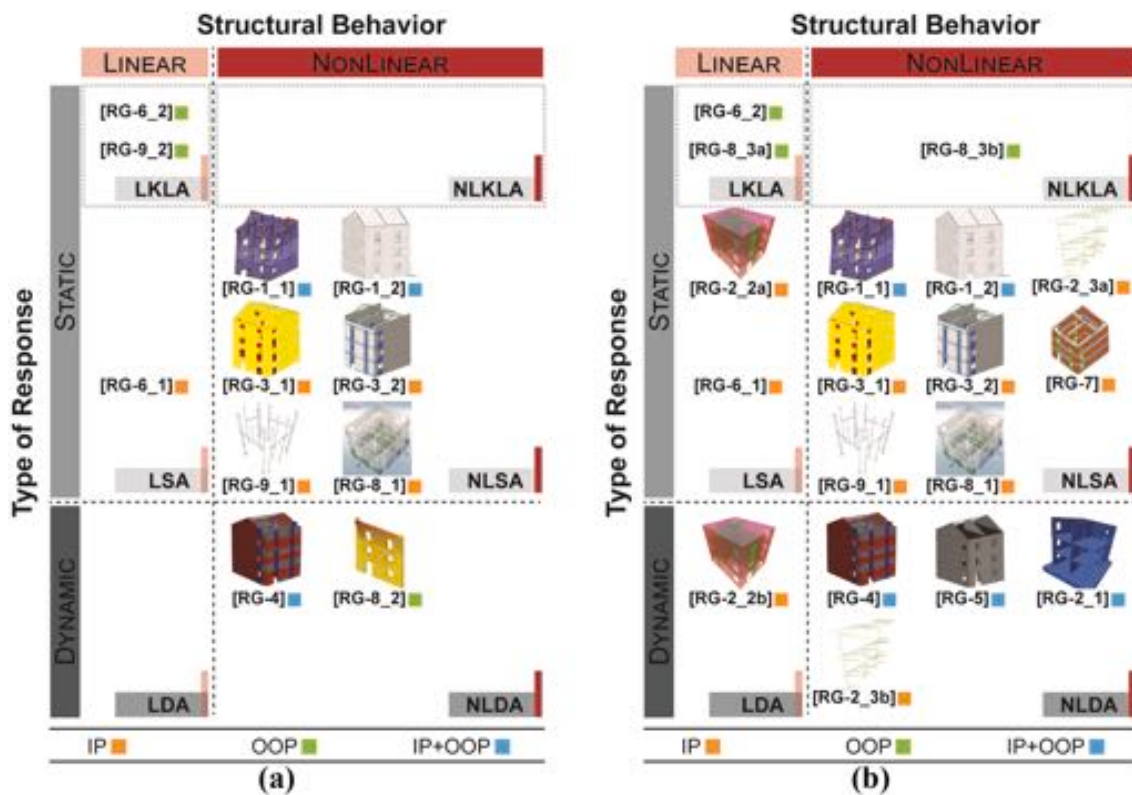N–M: plastic hinge coupling bending moment and axial load, M: flexural plastic hinge, L: link elements.

Fig. 8. Overview of methods of analysis adopted by the participating teams: (a) Case A and (b) Case B.

influence again the results, but their definition was reported just in two cases. RG-2 team adopted a mass proportional damping with 4% damping ratio for the brick masonry structure (Case B), while RG-4 team used Rayleigh damping, mass and initial stiffness proportional, with 3% damping ratio for the first mode and three times the value corresponding to this mode for both building configurations (Cases A and B). In this last aspect, there is some consensus in estimating the lower bound frequency for the calculation of Rayleigh damping parameters, but the selection of the higher bound frequency is less consensual, so resulting in additional variability.

The arbitrary definition of the representative point(s) of the building response was a source for higher dispersion of results, especially for Case A (with flexible horizontal diaphragms), in which different nodes were selected; see Tables 6 and 7. Considering the displacement of a single node or the average value from multiple points can further increase the arbitrariness. Since RG-9 team modeled the structure of Case A without floors, the resulting pushover curves are closely related to the response of each pier of the building measured at the corresponding control node at top level; see Table 7. Moreover, in NLDA the maximum displacement may not occur for the maximum base shear force, thus different approaches were defined, such as considering maximum or mean values (RG-2 team).

Regarding NLSA, the seismic action was generally applied in both main horizontal directions and positive/negative sign to consider its spatial variation [17], except for one case related to Façade 1 (RG-2 team). The lateral load distribution was in general assumed (by RG-2, RG-3, RG-7, RG-8 and RG-9 teams) with both "uniform", i.e. mass proportional, and "modal", i.e. proportional to 1st mode, patterns according to [17], while RG-1 team considered only the "uniform" pattern (Table 7). RG-7 and RG-9 teams have also performed the analysis considering the accidental eccentricity in both main directions.

5.2. Definition of limit state criteria

The differences in predictions of the seismic capacity of existing URM buildings can increase due to the definition of limit state criteria. In the blind prediction test, the minimum PGA_{NC} and PGA_{DL} were requested as synthetic parameters of the building response; see supplementary material. However, no criteria to define the attainment of these limit states was specified in the data provided to participants. Indeed, such definition may depend on the method of analysis and it results in different criteria according to the adopted design code (e.g. [3,63]) and/or the user judgment.

The proposed classification of criteria adopted by teams to define the attainment of NC limit state considering both IP and OOP mechanisms is presented in Table 8. Criterion 1 (C_{NC1}) is related to the reduction of the maximum base shear force from the pushover analysis. C_{NC2} defines the attainment of NC limit state as the first failure of one macro element, e.g. pier or façade wall. C_{NC3} is associated to convergence issues in the numerical simulation, which is hardly a sound criterion as it is also user or software dependent. NC condition for OOP mechanisms corresponds to the loss of static equilibrium according to C_{NC1} and C_{NC2} criteria.

A more detailed definition of each NC attainment criterion considered by the different teams is given in Table 9, in which this choice is also associated to the methods of analysis. It can be observed that, in the case of NLSA, C_{NC1} global criterion is the most frequent (RG-1, RG-3, RG-7 and RG-8 teams), while for NLDA local drift checks are performed at structural element level (C_{NC2}) by RG-2 and RG-4 teams.

The definition of each criterion for the attainment of DL limit state adopted by the few teams providing predictions is given in Table 10. Most teams (RG-1, RG-4 and RG-8) relate the DL attainment to interstory drift limits, but RG-6 team assumed the limit state once one pier of Façade 1 was damaged. In the column of OOP failure modes, the star refers to analysis considering only IP failure modes, while the hyphen states a combined approach (IP + OOP) in which a DL limit state criterion for OOP response is not available.
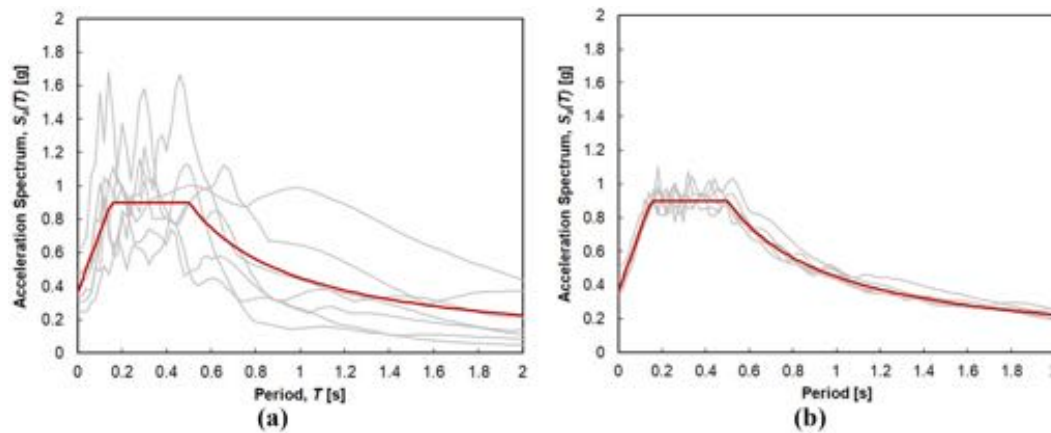
Fig. 9. Acceleration spectra of the selected accelerograms by teams (a) RG-4 and (b) RG-5, compared to Type 1 elastic response spectrum in Eurocode 8 Part 1 [17].

Table 6
Assumptions for nonlinear time-history analysis.

Approach	Cases	Combination of the effects of the horizontal components of the seismic action as in [17]	Time-history input signals	Representative point(s) of the building response
RG-2_1	B	–	7 synthetic accelerograms	Top nodes at the 4 corners
RG-2_3b	B (Façade 1)	–	7 synthetic accelerograms	Façade 1 central upper node
RG-4	A and B	–	7 natural accelerograms	Façades upper nodes
RG-5	B	✓	3 natural accelerograms	Top nodes of gables (Façades 2 and 3)
RG-8_2	A (Façade 1)	–	5 synthetic accelerograms	Façade 1 lateral upper node

Table 7
Assumptions for pushover analysis.

Team	Cases	Seismic actions	Lateral load pattern	Accidental eccentricity	Representative point(s) of the building response
RG-1	A and B	+long. and + transv. directions	Uniform (mass proportional)	–	Top nodes of gables in Façades 2 and 3 (A), centroid of top level (B)
RG-2	B (Façade 1)	+long. direction	Uniform and modal (1st mode proportional)	–	Façade 1 central top node
RG-3	A and B	±long. and ± transv. directions	Uniform and modal (1st mode proportional)	–	Nodes of walls at top level (A), centroid of top level (B)
RG-7	B	±long. and ± transv. directions	Uniform and modal (1st mode proportional)	✓	Nodes of walls at top level
RG-8	A and B	+long. and + transv. directions	Uniform and modal (1st mode proportional for A and B, plus linearly increasing along the height for B)	✓	Nodes of walls at top level (A), centroid of top level (B)
RG-9	A and B	±long. and ± transv. directions	Uniform and modal (1st mode proportional)	–	Nodes of walls at top level (A), centroid of top level (B)

6. Results of the predictions

Each participant team reported the minimum value of PGA$_{NC}$ and the associated failure mechanism, in addition to the adopted approaches for modeling and analysis. The following optional results were also requested, if available: range of variation of PGA$_{NC}$ obtained from different failure modes associated to IP and/or OOP responses, and value of PGA$_{DL}$. This section presents an overview of the obtained outcomes for Cases A and B, which will be compared to assess the dispersion resulting from the different choices as regards the modeling strategies and methods of analysis.

After the blind exercise, 11 and 16 predictions related to NC were collected from the involved teams for Cases A and B, respectively, while only 5 predictions related to DLs were received for Cases A and B; see Fig. 10. The total number of predictions differs for Cases A and B, and for NC and DL limit states, because the modeling of the two buildings and the consideration of the two limit states was constrained by the tools available to the different teams and/or by their numerical approaches. As stated, Case A represents a non-engineered existing building and the predictions at DL limit state may require additional checks, particularly regarding the OOP mechanisms, thus resulting in a lower number of predictions. Regarding the lower number of DL predictions, it is worth mentioning that only the ultimate states (i.e. NC or the life safety conditions) are mandatory in some codes, e.g. [46]. Most teams (7 out of 9) provided predictions associated to both IP and OOP responses, resulting from combined or sequential approaches (see Sections 4 and 5), with the exceptions of RG-3 team for Case A, and the RG-3, RG-7 and RG-9 teams

Table 8
Classification of criteria for NC limit state.

Limit state	C$_{NC1}$	C$_{NC2}$	C$_{NC3}$
NC	Reduction of base shear capacity and loss of equilibrium	Failure of one macro element and loss of equilibrium	Lack of convergence

for Case B. For this last building configuration (Case B), some teams neglected the OOP mechanisms because of given structural details, i.e. presence of systematic RC tie beams and rigid floors, which allow to assume the box-like behavior, also applicable in design of new buildings.

Table 9
Criteria for defining NC limit state for each team.

Team	Failure modes		Criterion	Analysis method
	IP	OOP		
RG-1	20% reduction of base shear capacity / lack of convergence		C_{NC1}, C_{NC3}	NLSA
RG-2	Façade 1 becomes unstable (SEM) and lack of convergence (DIM)		C_{NC2}, C_{NC3}	NLSA and NLDA
RG-3	20% reduction of base shear capacity		C_{NC1}	NLSA
RG-4	One pier reaches the drift limits of 1.0% for flexure and 0.7% for shear (Case A), and 0.8% and 0.4% for Case B	Loss of static equilibrium	C_{NC2}	NLDA
RG-5	Lack of convergence		C_{NC3}	NLDA
RG-6	Failure of all piers in Façade 1	Loss of static equilibrium of gables in Façades 2 and 3	C_{NC2}	LSA and LKLA
RG-7	50% reduction of base shear capacity		C_{NC1}	NLSA
RG-8	20% reduction of base shear capacity	Loss of static equilibrium	C_{NC1}	NLSA and NLDA (A) NLSA and L/NLKLA (B)
RG-9	One pier reaches the drift limits of 0.6% for flexure and 0.4% for shear	Loss of static equilibrium	C_{NC2}	NLSA and LKLA (A) NLSA (B)

Table 10
Criteria for defining DL limit state for each team.

Team	Failure modes	
	IP	OOP
RG-1	Inter-story drift of 0.3%	&
RG-4	Inter-story drift of 0.2%	Crack width reaches 2 mm
RG-6	Failure of one pier in Façade 1	*
RG-8	Inter-story drift of 0.3%	*

& combined approach (IP + OOP) with OOP criterion not available.
* only IP approaches.

6.1. Case A: Comparison of failure modes and capacity curves

The building configuration for this Case (A) presents intrinsic vulnerabilities potentially leading to both IP and OOP failure mechanisms, which are strictly governed by the modeling assumptions; see Section 4. Indeed, the seismic behavior of this building is highly influenced by the type of horizontal diaphragms and the lack of tie rods; see Section 3. In the following, the predicted failure modes are briefly reported and compared to evaluate their consistency, as well as the capacity curves available from pushover analysis.

The reported failure mechanisms were classified according to the related IP or OOP modes of specific structural components (Fig. 11). Reference is made to the modeling strategy, method of analysis and failure modes, even if the corresponding picture is not available. Most predictions showed significant damage in the unloaded Façades 1 and 4, as well as in the gables of Façades 2 and 3. In particular, predicted damage of Façade 1 included: diagonal cracking for all piers at the ground floor (RG-6); diagonal cracking and rocking mechanisms of piers at the ground and 1st levels (RG-1_1); widespread rocking of piers at the building base and of spandrels at each level (RG-8_1). These mechanisms were grouped into the class of IP failure modes of Façade 1 at ground floor. When the predicted IP mechanisms refer to rocking of piers/spandrels at the 2nd level, they fall into class IP failure modes of Façade 1

at 2nd floor, namely for both models by RG-3 team with flexural and shear mechanisms respectively shown at the left and right sides of Fig. 11. Contrarily, RG-9 team foresaw the longitudinal internal wall as the critical one, with rocking developed at the base of each pier. This was included into a specific class in Fig. 11.

The lack of tying elements at the top level resulted in predictions of overturning of the upper wall of Façade 1 (RG-4 and RG8_2) or Façade 4 (RG-1_2), in which also a mixed mechanism with overturning and horizontal arching was foreseen by RG-1 team; see Fig. 11. Neglecting the restraint of tie rods, orthogonal walls and floors by RG-9 team resulted in the overturning of the central wall of Façade 1. The overturning of gables in Façades 2 and 3 is likely to occur due to the pounding of timber struts, as confirmed by the prediction of several teams (RG-1, RG-4 and RG-6). In general, OOP mechanisms activate first than IP ones for Case A if a combined approach (IP + OOP) or a sequential one (firstly IP, then OOP, or vice-versa) is considered; see Fig. 11. Moreover, the assumption of the most critical elements (i.e. base piers of Façade 1 and gable walls in Façades 2 and 3) by RG-6 team is consistent with the predictions of other teams.

The capacity curves provided by the participating teams that performed pushover analysis have been compared to evaluate their differences in terms of initial stiffness, maximum value of base shear force (V_{max}) and displacement capacity, which are presented in Fig. 12 for the longitudinal and transversal directions. Each prediction is labeled with an aleatory number and the corresponding load pattern to avoid any reference to teams and software used by them. Since no information about weight of the building and height of control points was provided, the results are not presented in terms of load factor and drift ratio. In any case, the set of capacity curves evidences a huge scatter.

The arbitrariness in modeling the effect of cracking can result in different initial stiffness values of the predicted capacity curves, which are given in Table 11. The reported values were calculated as the secant stiffness at 15% of V_{max} and, when considering both the positive and negative senses, an average stiffness is computed if $|V_{max}| \neq |-V_{max}|$. The dispersion is given as percentage difference from the mean stiffness in the longitudinal or transversal directions, $\bar{k}_{long, CaseA}$ or $\bar{k}_{transv, CaseA}$, regardless of the adopted load pattern. If specific force–drift relations with stiffness degradation are not adopted, the elastic modulus should be reduced to account for this phenomenon, typically 50% of the stiffness of uncracked elements [17]. Although this information was not reported by each team, it may be implicitly assumed (except by RG-2 team) for all the predictions considering Eurocode 8 Part 1 [17] or NTC 2008 [63] as reference building codes. A comparable initial stiffness is observed, especially between curves 3, 4 and 5 for a same load pattern in Fig. 12a and Table 11. The variation reduces for these curves in the transversal direction (Fig. 12b), but the differences in V_{max} are significant (up to 120% when using the average value as reference). The structure presents lower stiffness and force capacity in the longitudinal direction and for modal load pattern, mainly because of the lower wall density and limited floor weight on piers. The lowest capacity in terms of force is for curve 5 in Fig. 12, mostly due to the modeling assumption of spandrels with brittle behavior. Curves 1 and 2 in Fig. 12a, which were obtained from a combined IP + OOP approach, denote a base shear capacity similar or even lower than those resulting from IP approaches, because OOP mechanisms limit the global capacity. However, the differences in the initial stiffness associated to these curves are significantly high (up to 150% of $\bar{k}_{long, CaseA}$), possibly due to different assumptions in the conventional coefficients assumed to simulate the stiffness degradation phenomena associated to the damage for flexural and shear behavior. As mentioned before, these coefficients correspond to the reduction of 50% of the stiffness related to both flexural and shear contributions in uncracked structural elements. However, in some cases, only the stiffness reduction for shear damage is considered, so assuming that the degradation associated to the flexural behavior may be captured directly by the model (e.g. when a fiber approach or other more refined
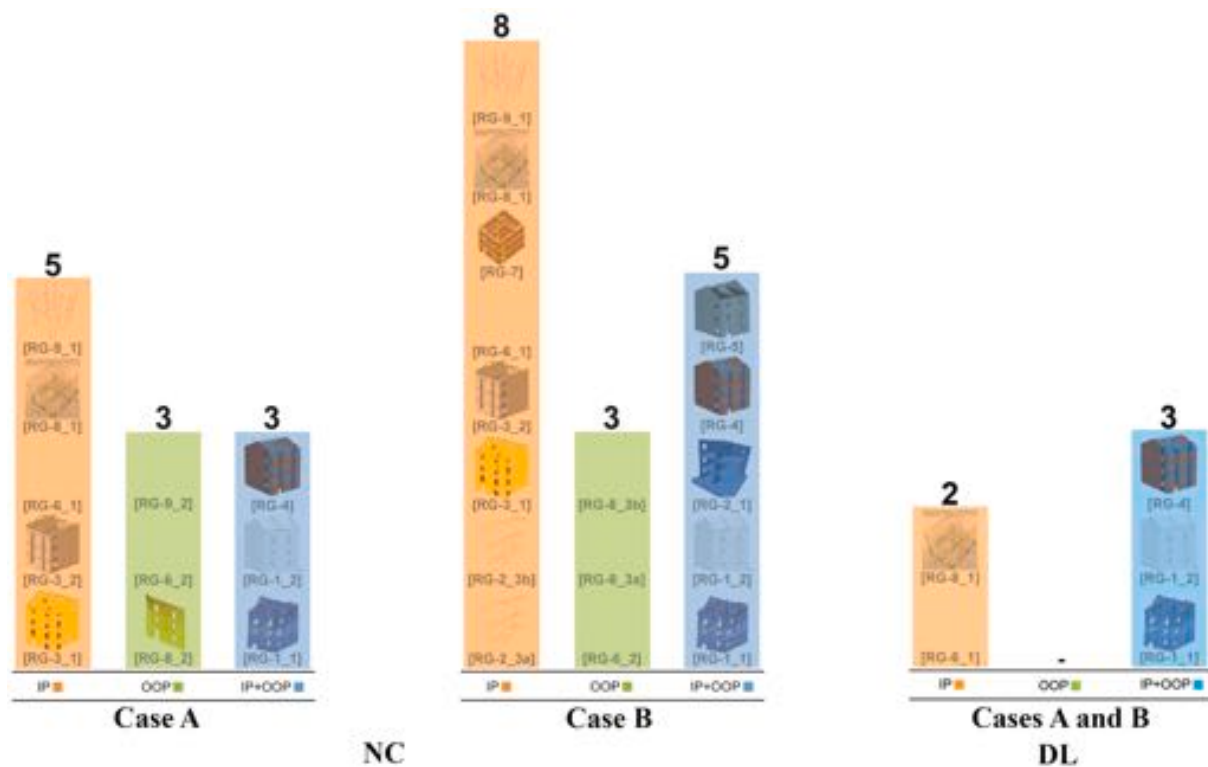
Fig. 10. Number of predictions provided by teams for the considered case studies and limit states.

solution is adopted).

Since the displacement capacity is usually determined based on the 20% reduction of base shear strength [17], it cannot be calculated from all curves because the softening branches are not fully developed due to missing convergence or the fact the curves were reported only until this point. Still, the difference in maximum displacement is significant among the curves. Yielding occurs around 5 mm for curves 1, 2 and 5, and 10 mm for curves 3 and 4 in both directions (Fig. 12). A sudden vertical drop of V_{max} is observed especially for curves 3 and 4. The differences are also due to the selection of control points whose definition was not similar among teams, since Case A presents flexible timber diaphragms; see Section 3.

6.2. Case B: Comparison of failure modes and capacity curves

The building structure for this Case (B) is expected to exhibit more global behavior than the one of Case A due to the good bond of its brick masonry, the presence of RC horizontal diaphragms and RC tie beams, and effective connections. These features ensure that the IP response of walls will be mobilized, even if OOP mechanisms can still potentially occur in the upper parts of the external façades. The consideration of these mechanisms in the numerical models depends on the assumptions for the wall-to-roof connection. The results for Case B are presented consistently with the organization of the previous section for Case A, in terms of predicted failure modes and capacity curves.

Although there are some differences in terms of predicted failure modes and their extent between the two configurations, these modes are still classified according to the classes defined for Case A in Subsection 6.1. Two additional classes were considered, i.e. IP failure mode of Façade 1 related to rocking of piers at the building base and diagonal sliding of upper spandrels, and IP mechanisms of Façade 2/3 at ground floor. Many predictions for Case B show the sliding shear failure of piers as the most likely damage scenario for Façade 1, rather than flexural failures. While in Case A it was in general predicted that Façades 2 and 3 would not be heavily damaged, in Case B it was foreseen that they would

present severe horizontal and diagonal sliding mechanisms at the ground floor.

OOP collapses of the upper parts of Façades 1 and 4 were predicted just in two cases (by RG-1 and RG-4 teams), while, for Case A, they were always foreseen when using a combined IP + OOP approach. The global behavior in Case B is also demonstrated by the damage pattern of all walls in the longitudinal direction, which is compatible with a global rocking mechanism of the building, as exemplified in Fig. 13, according to the prediction by RG-1 team.

The IP failure mechanisms are also in this case diagonal sliding of piers in Façade 1 at the ground floor as predicted by RG-4, RG-6 and RG-7 teams. This diagonal sliding is combined with rocking of piers in the predictions of RG-2 and RG-3 teams; see Fig. 14. However, the estimation by RG-9 team showed the longitudinal internal wall as the most critical in the building, with rocking of each pier at the ground floor as in Case A; see Subsection 6.1. The same wall presents, according to the prediction of RG-1 team, damage by diagonal sliding combined with rocking (Fig. 13b). RG-4 team foreseen also large deformations at upper elements together with gable overturning in Façades 2 and 3.

Based on incremental nonlinear time-history analyses, RG-2 team predicted horizontal sliding of the upper piers and diffused diagonal sliding of spandrels, together with rocking of the base piers of Façade 1. The damage of spandrels was foreseen by RG-5 team as well; see Fig. 14. According to the predictions of RG-1 and RG-8 teams, Façades 2 and 3 show diagonal sliding shear of the long pier at the ground floor. This failure mode was also predicted by RG-3 team, combined with rocking of the small pier at the ground and 1st floors, and with diagonal sliding of the transversal internal wall at ground level. RG-9 team reported the rocking failure of both walls at the base of Façades 2 and 3.

OOP mechanisms are still possible with overturning of the upper part of Façade 1 or Façade 4, as predicted by RG-4 and RG-1 teams, respectively, or overturning of the gables of Façades 2 and 3 according to RG-1, RG-4 and RG-8 teams. A mixed vertical and horizontal arching mechanism of the upper part of Façade 4 was also predicted by RG-5 team because of the presence of a physical gap between stairs and side
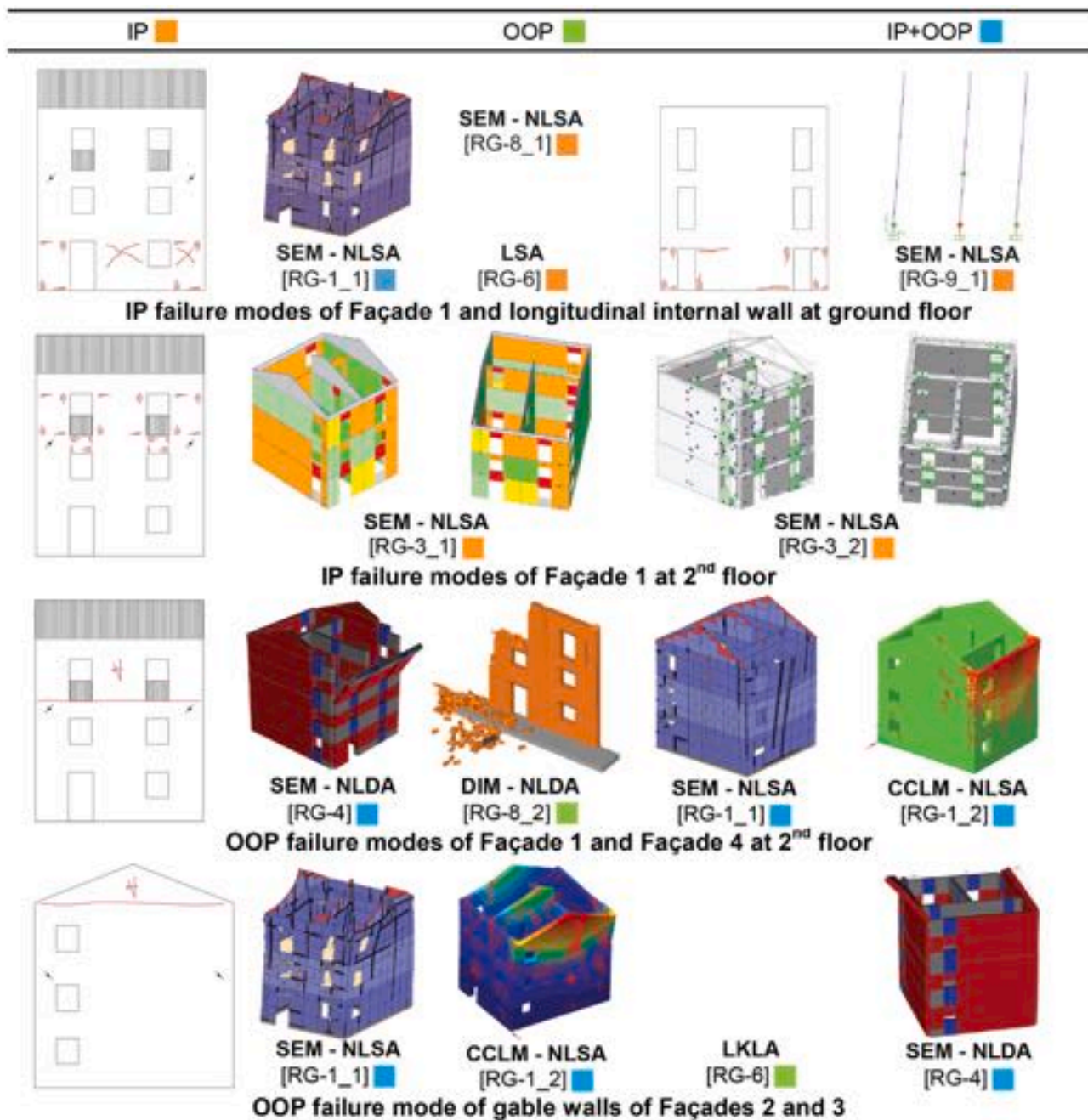
Fig. 11. Classification of predicted failure modes for Case A.

walls; see Subsection 4.2 and Fig. 14. This was still classified in the same class, although the OOP mechanism is a combination between horizontal and vertical arching.

The same comparison made in Subsection 6.1 between capacity curves is made for Case B in Fig. 15a–b for the longitudinal and transversal directions, respectively, and in Table 12 for the corresponding initial stiffness, again with unacceptable scatter. The building still presents lower stiffness and V_{max} in the longitudinal direction and for modal loading (1st mode proportional), but the differences in terms of initial stiffness and V_{max} are larger than in Case A. These results were unexpected since Case B represents a code-based existing building, with its seismic response mainly controlled by the IP behavior of masonry walls. This is true especially when assuming floors as rigid diaphragms and a good wall-to-wall connection, able to activate the flange effect. Both aspects may alter in a significant way the load redistribution among

walls in the linear and nonlinear fields. This is why the modeling of heavy and stiff floors and the coupling among walls with different approaches may result in a not negligible dispersion of predictions. Indeed, the global response of the building depends on the capacities of the masonry panels, which are much affected by the axial load acting on them.

The largest differences are for curves 1 and 2 corresponding to uniform loading, i.e. up to 180% of $\bar{k}_{long,\,CaseB}$, which were obtained considering a combined IP + OOP approach. The range of variation significantly reduces if only curves 3–7 are compared against the absolute differences of V_{max} (127% when considering the average value as reference) and of initial stiffness (up to 78% of $\bar{k}_{long,\,CaseB}$) similar to those of Case A (120% and 55%, respectively). The lower initial stiffness of curve 6 in Table 12 is related to the assumption of larger effective height of unconfined external piers, so smaller rigid nodes at their ends,
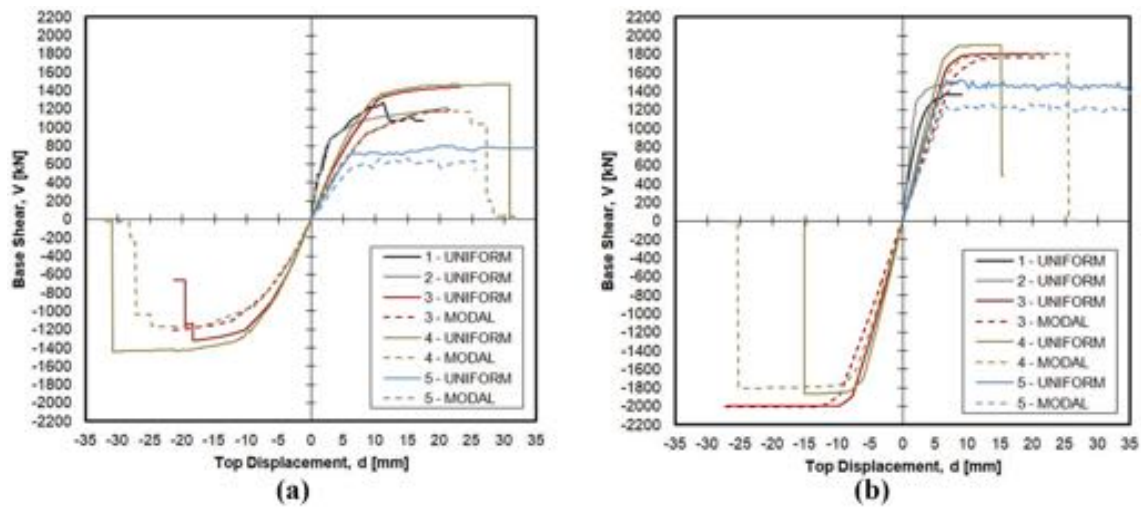
Fig. 12. Capacity curves in (a) longitudinal and (b) transversal directions for Case A.

Table 11
Initial stiffness of pushover curves for Case A.

Curve tag	Load pattern			
	Uniform		Modal	
	k_{long} [kN/m]	k_{transv} [kN/m]	k_{long} [kN/m]	k_{transv} [kN/m]
1	487,645 (150%)	650,193 (108%)	–	–
2	389,146 (100%)	650,193 (108%)	–	–
3	170,575 (−12%)	258,425 (−17%)	141,037 (−28%)	214,298 (−31%)
4	177,219 (−9%)	291,383 (−7%)	142,825 (−27%)	238,764 (−24%)
5	108,680 (−44%)	259,268 (−17%)	87,273 (−55%)	188,675 (−40%)

Mean values: $\bar{k}_{long,\,CaseA} = 194,672\ kN/m$; $\bar{k}_{transv,\,CaseA} = 312,839\ kN/m$.

as well as the associated lower V_{max} of the building is related with the limited drift capacity of the adopted plastic hinges at the piers. Regarding the displacement capacity, the structure fails around 15–20 mm at curves 2, 3, 4 and 7 for both directions (Fig. 15). A lower ductility is observed when compared with Case A, due to the more brittle behavior of the activated shear sliding failure mechanisms.

6.3. Comparison of predicted PGAs

The minimum PGAs associated to the failure mechanisms at NC limit

state described in Subsections 6.1 and 6.2, as well as those at DL limit state were compared to assess the dispersion of results in the blind prediction test. This dispersion is calculated as a percentage difference from the mean PGA value provided by the different teams, regardless of failure mechanisms, modeling strategies, methods of analysis and definition of limit state criteria. The differences are reported and commented without any reference to teams and software used by them, thus using a random numbering from 1 to 9.

The predicted values of PGA_{NC} are scattered for both configurations, ranging from 0.064 g to 0.32 g in Case A, and from 0.12 g to 0.59 g in Case B; see Table 13. The mean values are 0.19 g for Case A and 0.28 g for Case B, with standard deviations (and coefficients of variation, CoV) of 0.084 g (45%) and 0.16 g (58%), respectively. Both minimum and maximum $PGAs_{NC}$ for Case B are almost twice the ones for Case A, while the CoVs are not so different (excessively high in any case). This is consistent with the fact that Case A was expected to be more vulnerable than Case B, but, as stated before, more homogenous values were expected in Case B. The minimum value of $PGA_{NC,\,min}$ for Case A results from a different schematization of the building, which was modeled as a series of cantilever piers, whose horizontal displacement is coupled at floor level by means of truss elements. This may represent the lower bound for Case A, with no diaphragms (see Subsection 4.3).

The percentage differences of predicted PGA_{NC} values from their mean value for each building configuration are shown in Fig. 16. Two predictions for both configurations exceed the threshold of the mean value plus/minus the standard deviation, with a maximum distance to the average of 111% and 72% of the standard deviation for Cases B and A, respectively. Unexpectedly, 4 predictions out of 9 for Case A present a difference from the $PGA_{NC,\,mean}$ lower than 5%, while just one is within
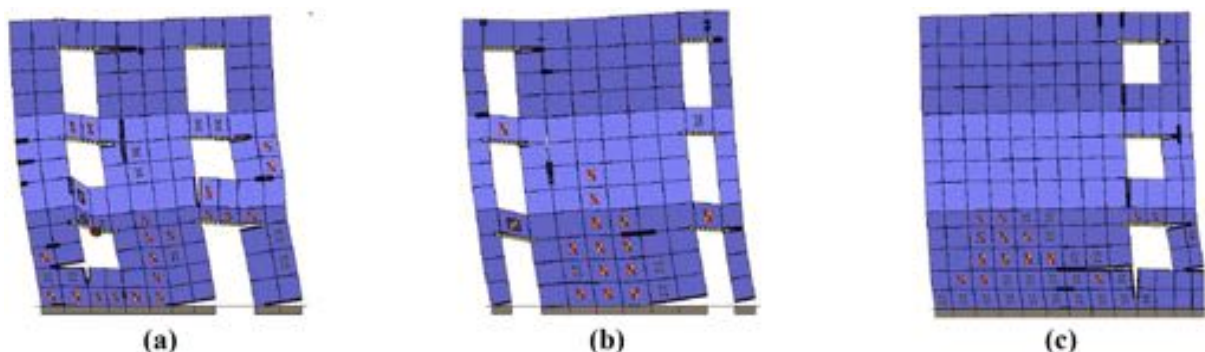

Fig. 13. Damage predictions by RG-1 team in the longitudinal direction: (a) Façade 1, (b) internal wall and (c) Façade 4.
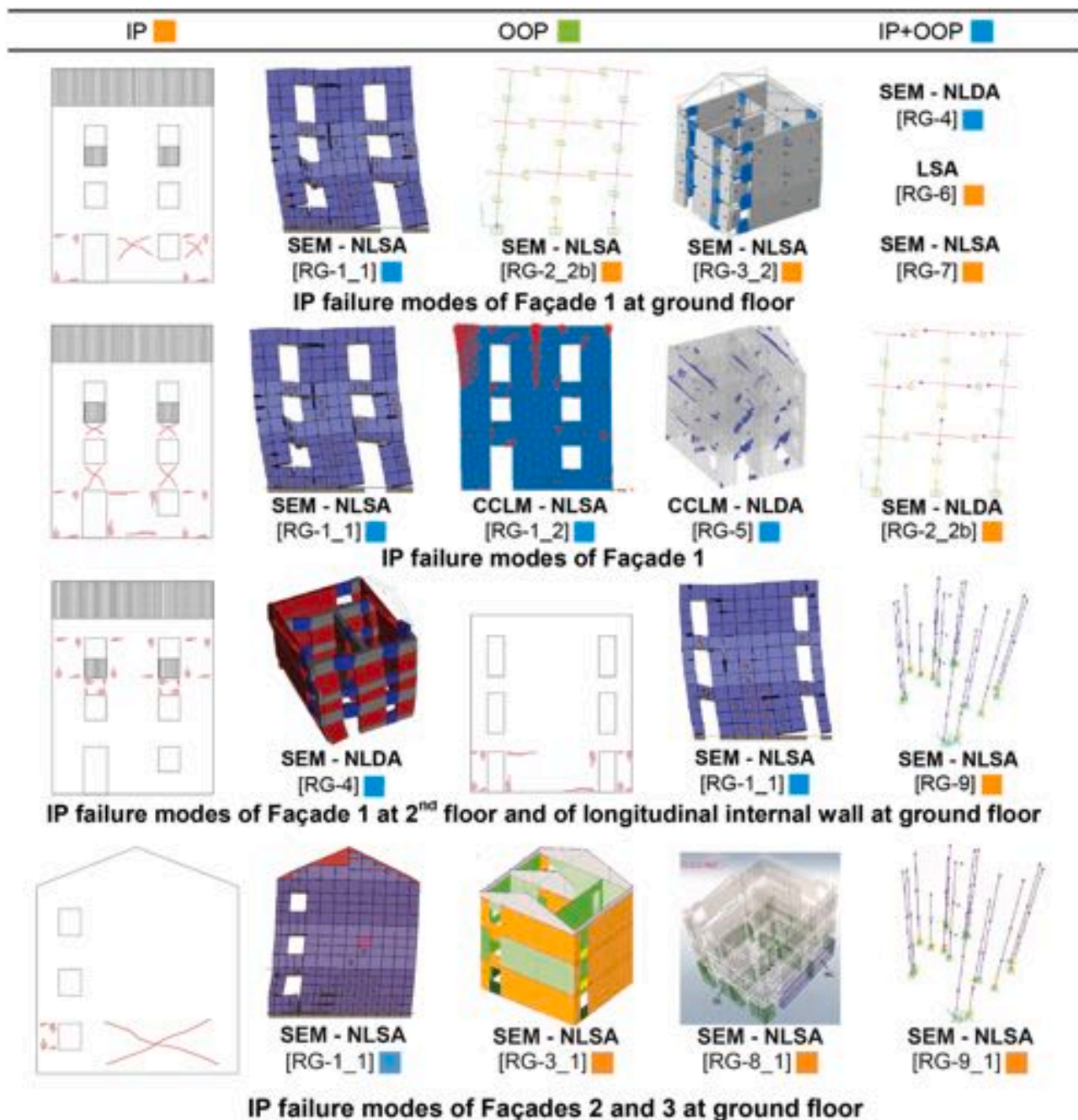
Fig. 14. Classification of predicted failure modes for Case B.

this range for Case B.

Regarding the predictions related to DL limit state, the values of PGA_{DL} range from 0.075 g to 0.27 g in Case A, and from 0.12 g to 0.48 g in Case B. Despite the number of predictions is small and the statistic sample is not significantly representative, the mean values are 0.15 g for Case A and 0.25 g for Case B, with standard deviations (and CoVs) of 0.087 g (58%) and 0.16 g (65%), respectively. A trend similar to the one for the NC predictions is shown in Fig. 17 in terms of maximum differences (80% and 93% of the standard deviation for Cases B and A, respectively) and one PGA_{DL} for each building case exceeding the threshold of the mean value plus/minus the standard deviation.

Each prediction is related to a given approach in terms of considered failure mechanisms (IP, OOP, IP + OOP), modeling strategies (DIM, CCLM, SEM and MBM), methods of analysis (LKLA, NLKLA, NLSA,

NLDA) and limit state criteria (C_{NC1}, C_{NC2} and C_{NC3}); see Sections 4 and 5. Thus the PGA values were grouped to be compared among the considered classes of approaches. In this case, the trend of standard deviations among classes is more representative than the difference from the PGA_{mean} because this difference depends also on the number of predictions for each class against the total ones. For the sake of clarity, this number is given in brackets for all the classes, e.g. IP (5).

The percentage differences of NC predictions per failure mode from the reference $PGA_{NC, mean}$ values (i.e. 0.19 g and 0.28 g for Cases A and B, respectively), as well as the standard deviations for each class (highlighted with a red dash-dot line), are shown in Fig. 18. The values for Cases A and B are comparable, with lower differences for the IP and OOP classes of mechanisms, and presenting a larger difference for the IP + OOP class. The trend of standard deviations is similar for both Cases A
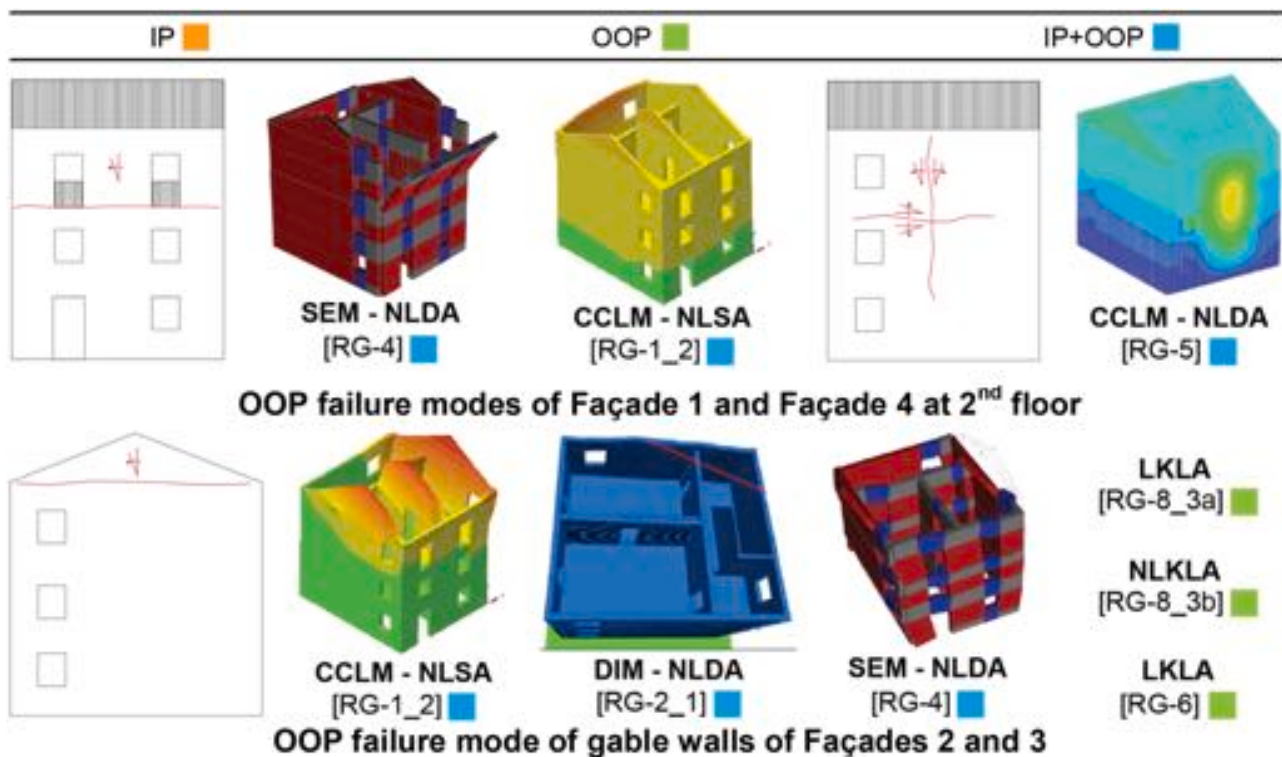
OOP failure modes of Façade 1 and Façade 4 at 2nd floor

OOP failure mode of gable walls of Façades 2 and 3
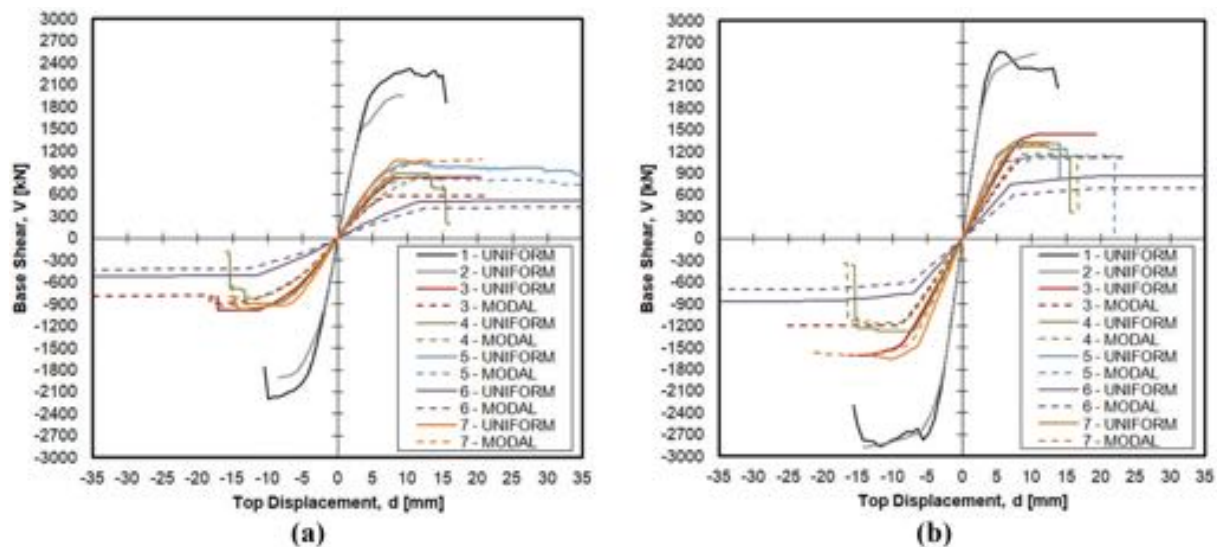
Fig. 14. (*continued*).

Fig. 15. Capacity curves in (a) longitudinal and (b) transversal directions for Case B.

and B, with a narrowing of the scatter for the OOP class and a fully positive scatter domain of predictions for the IP + OOP class. A wide deviation range is observed in Fig. 18b for Case B, thus the dispersion is still large even considering the same type of failure modes.

When the predictions are grouped according to the modeling strategies presented in Section 4, the lowest differences occur for DIM, SEM and MBM in Case A, and for SEM in Case B, as shown in Fig. 19. Since the reference PGA_NC, mean value for Case A results from most predictions obtained by approaches using SEM, the difference related to this modeling class is almost zero (–2%), but the deviation is quite large (±41%). The same consideration applies to Case B, although there are more predictions resulting from modeling strategies others than SEM

when compared to Case A, i.e. 5 against 3. The largest difference in Case B is observed for CCLM class, with its PGA_NC value exceeding the reference standard deviation (±58%) and presenting a wide deviation range (118%) due to the different limit state criteria. The minimum deviation range corresponds to MBM class in Case B, also because the relating predictions resulted from the same team.

Regarding the predictions grouped according to methods of analysis presented in Section 5, the most representative samples are those related to nonlinear analyses, both static and dynamic (7 and 2 out of 11 for Case A, and 9 and 4 out of 16 for Case B, respectively); see Fig. 20. Although the difference for NLSA is small for Case A (7%), the class-related standard deviation exceeds the reference deviation (±45%

Table 12
Initial stiffness of pushover curves for Case B.

Curve tag	Load pattern			
	Uniform		Modal	
	k_{long} [kN/m]	k_{transv} [kN/m]	k_{long} [kN/m]	k_{transv} [kN/m]
1	519,344 (179%)	700,243 (164%)	–	–
2	520,364 (180%)	719,032 (171%)	–	–
3	126,429 (−32%)	177,103 (−33%)	103,010 (−45%)	143,541 (−46%)
4	135,546 (−27%)	187,242 (−29%)	107,454 (−42%)	150,579 (−43%)
5	173,559 (−7%)	234,295 (−12%)	168,600 (−26%)	192,087 (−28%)
6	54,368 (−71%)	107,681 (−59%)	41,265 (−78%)	81,983 (−69%)
7	146,831 (−21%)	232,838 (−12%)	137,204 (−26%)	202,225 (−24%)

Mean values: $\bar{k}_{long, CaseB} = 186,158 \, kN/m$; $\bar{k}_{transv, CaseB} = 265,060 \, kN/m$.

Table 13
Statistical data of the predictions at NC limit state.

Case	$PGA_{NC, min}$ [g]	$PGA_{NC, max}$ [g]	Difference [g]	$PGA_{NC, mean}$ [g]	CoV [%]
A	0.064	0.32	0.26	0.19	45
B	0.12	0.59	0.47	0.28	58

and ± 58% for Cases A and B, respectively) indicating a large dispersion of results. This dispersion resulted from the arbitrariness in the modeling and representation of the seismic action by teams as presented in Sections 4 and 5. For NLDA, the difference as well as the deviation range are lower (Fig. 20a). A similar trend is observed in Fig. 20b for Case B in terms of deviation range, but in an opposite order when compared to Case A, i.e. difference of 22% for NLSA and 36% for NLDA. As expected, the $PGAs_{NC}$ for LKLA and NLKLA classes are lower than the reference $PGA_{NC, mean}$ (i.e., −31% and −36% in Case B, respectively) because they are related to the OOP mechanism of gable overturning whose vulnerability is expected to be even larger. The same consideration applies to the overturning of Façade 1 for Case A, in which the $PGAs_{NC}$ for LKLA is 39% less than the reference $PGA_{NC, mean}$ (0.19 g).

Eventually, the predicted PGA values were grouped based on the proposed classification of NC criteria presented in Subsection 5.2. A similar trend is shown in Fig. 21 for Cases A and B: the PGA_{NC} values for criteria C_{NC1} and C_{NC2} are close to the reference $PGA_{NC, mean}$ value, but, for Case B, the deviation range is larger. More scattered results can be observed for criterion C_{NC3} because its definition is related with computational convergence, so having no physical meaning.

The predicted $PGAs_{DL}$ were also grouped according to the previous classes, but the number of predictions limits the reliability of a statistical analysis. Still, a similar trend of dispersion and deviation ranges among Cases A and B was observed for the considered classes of approaches in terms of failure modes, modeling approaches and methods of analysis. In particular, the minimum differences were noticed for the classes IP, SEM and LKLA, respectively. The maximum difference is for CCLM approach with a deviation of 80% and 93%, respectively from the reference $PGA_{DL, mean}$ values for Cases A and B (0.15 g and 0.25 g, respectively). The dispersion of results for DL limit state is also confirmed by the large deviation ranges of predictions considering IP + OOP mechanisms, and using SEM and NLSA.

7. Conclusions

A benchmarking of procedures for seismic vulnerability assessment of URM buildings is presented in this paper with reference to a blind prediction test organized within a Special Session at the European Conference of Earthquake Engineering Series. An overview of the procedures adopted by nine participating teams is given to highlight the open issues and arbitrariness in using different modeling approaches, methods of analysis and definitions of limit state attainment. The blind predictions from each team are compared in terms of minimum PGA values associated to the potential failure mechanisms at NC limit state. The available results regarding the DL limit state are also compared, even if statistically less significant.

The case studies are two typical configurations representing non-engineered and code-based designed buildings, namely: Case A) stone masonry walls with flexible timber floors; and Case B) brick masonry walls with rigid RC slabs. The structures were idealized so that the participating teams had to resort to expert judgment when performing the seismic assessment through different modeling approaches and methods of analysis. The approaches were described to allow comparing and unveiling the dispersion between predictions. Arbitrariness in choices is larger in Case A than in Case B, because of given construction details which influence the seismic behavior of the buildings at both local and global levels. In particular, the limited IP stiffness of timber
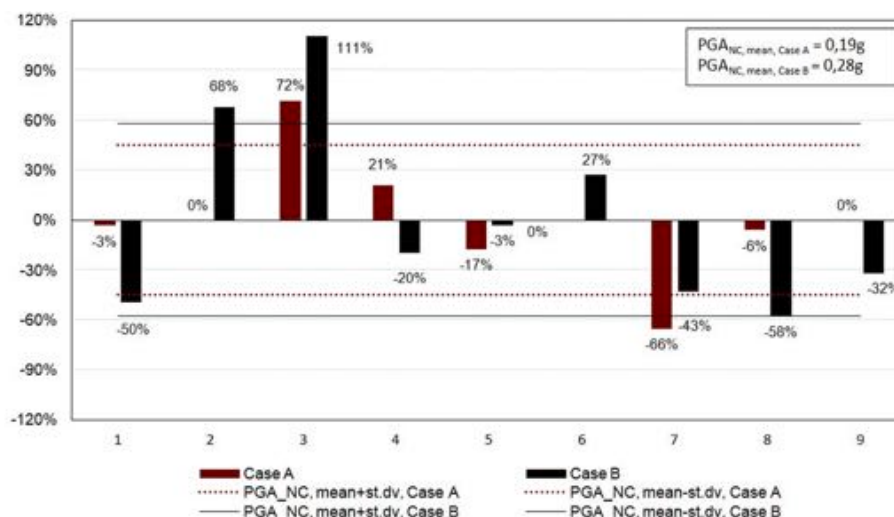

Fig. 16. Differences in NC predictions from the mean values per building configuration.
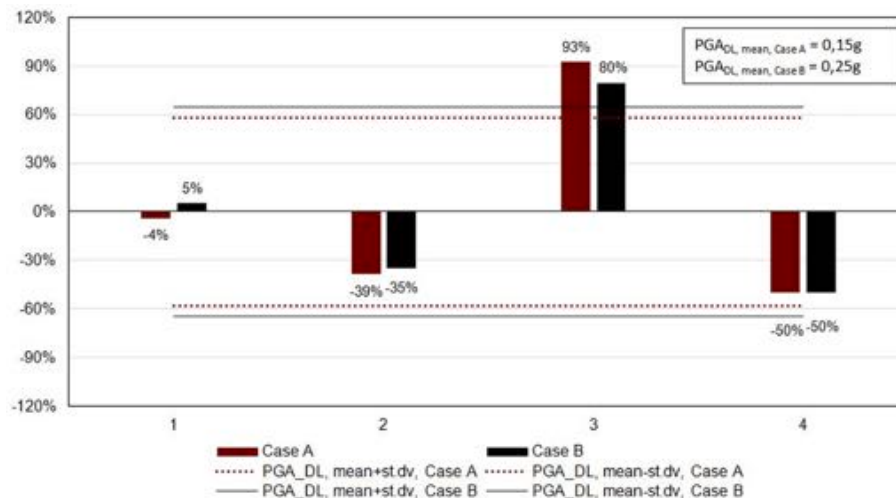
Fig. 17. Differences in DL predictions from the mean values per building configuration.

floors and the partial coupling between walls in Case A leads to a larger range of assumptions than in Case B. A box-like behavior can be assumed for Case B, mostly controlled by the IP response of the walls.

The predicted failure modes among teams show a good agreement for both Cases A and B, and they are consistent with those expected for buildings with similar structural characteristics. Predictions for Cases A and B show the main façade of the buildings as the most vulnerable element. Although OOP mechanisms of gables and upper walls are common to both Cases A and B, some differences were observed for the IP modes, with a prevalence of diagonal and sliding shear mechanisms, as well as more severe damage for the side façades in Case B.

When the attention is focused on the obtained capacity curves, the predictions result in larger differences for Case B than for Case A, in terms of initial stiffness, yield point, base shear strength and displacement capacity, despite Case B represents a code-based building. Since there is no experimental test for cross-validating the results, the reliability and accuracy of the predictions are assessed based on the qualitative estimate of damage patterns against real damage evidence in existing buildings with similar vulnerabilities, when comparing the outcomes obtained from the different software packages and approaches. If only the predictions related to IP failure mechanisms are considered, the range of variation drops to differences comparable to those for Case A, which are still large (i.e. a range of 120% of the average value for the maximum shear force). Case B presents a relatively lower displacement capacity than Case A (15–20 mm against 20–30 mm,

respectively), due to a sequence of similar shear failure mechanisms, so with limited possibility of lateral force distribution.

The minimum values of PGA_{NC} obtained by each team were compared to calculate their difference from the mean PGA value computed by considering all the predictions (0.19 g and 0.28 g for Cases A and B, respectively). The higher scatter of the $PGAs_{NC}$ was for Case B (from 0.12 g to 0.59 g) because of the larger number of predictions, but also due to significant differences among approaches in considering IP and combined IP + OOP mechanisms. However, the range of variation is also wide in Case A, ranging from 0.064 g to 0.32 g. The same considerations apply for the results corresponding to the DL limit state, despite the limited number of predictions. The dispersion is also due to different criteria in defining the attainment of each limit state condition. A comparison of PGAs was also made by grouping the predictions into comparable classes with respect to failure modes, modeling strategies, methods of analysis and limit state criteria.

Additional analyses of both buildings are required to assess their actual seismic capacity and further understand the influence of each given assumption (about modeling approaches, methods of analysis, and criteria to define limit states) on the results, since this was not in the scope of the exercise. Indeed, the provided data and required results in the blind prediction test were not intended to investigate the weight of sources of dispersion, and so the comparisons are inconclusive whether one choice has higher effects on the predicted PGA among all the alternatives. Moreover, all assumptions and all predictions made by
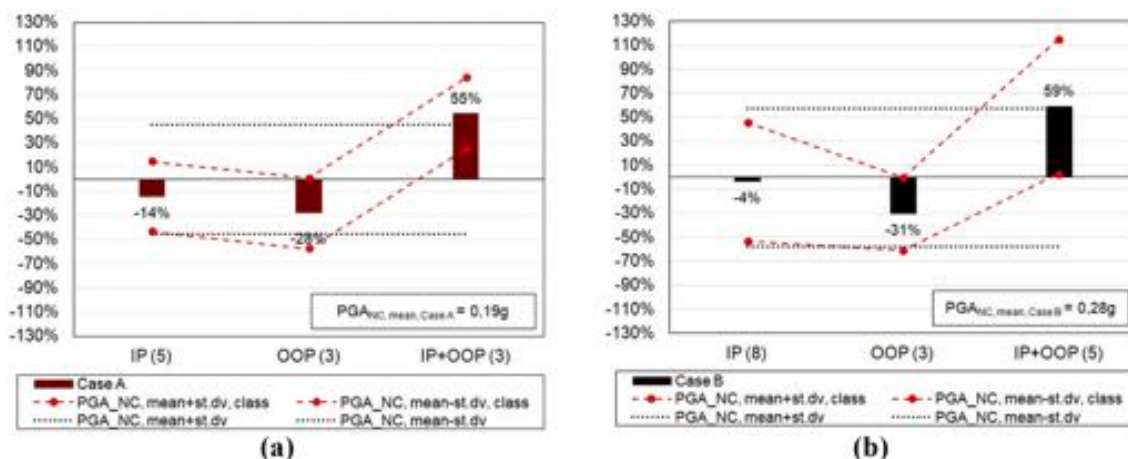

Fig. 18. Differences in NC predictions per failure mode for (a) Case A and (b) Case B.
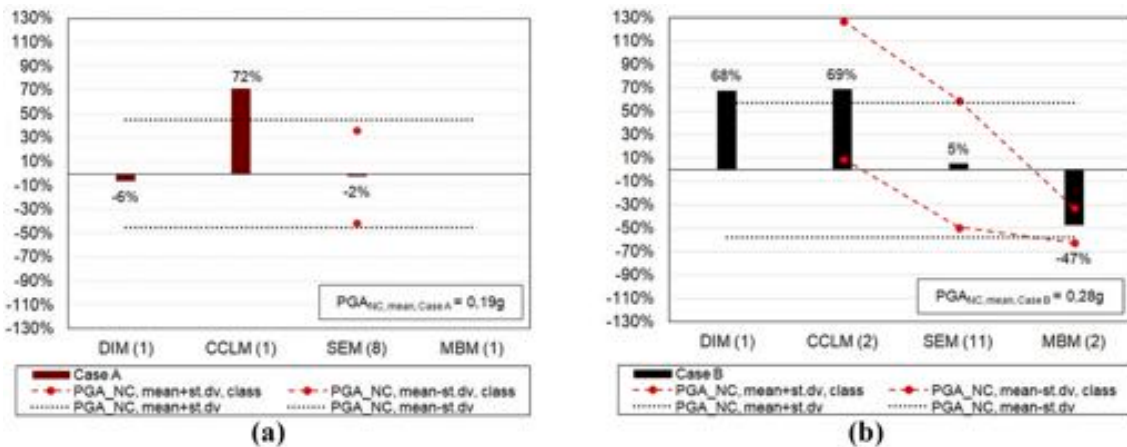
Fig. 19. Differences in NC predictions per modeling approach for (a) Case A and (b) Case B.
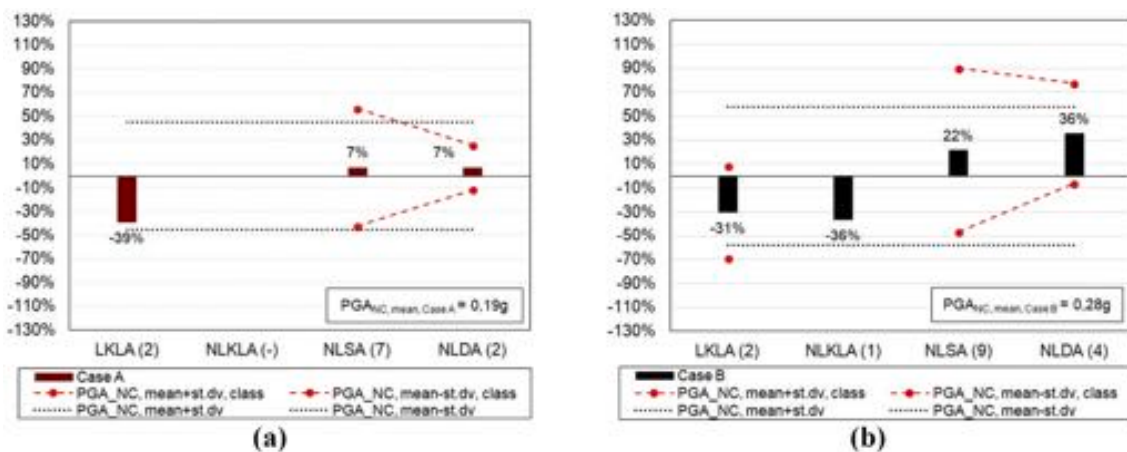

Fig. 20. Differences in NC predictions per analysis method for (a) Case A and (b) Case B.
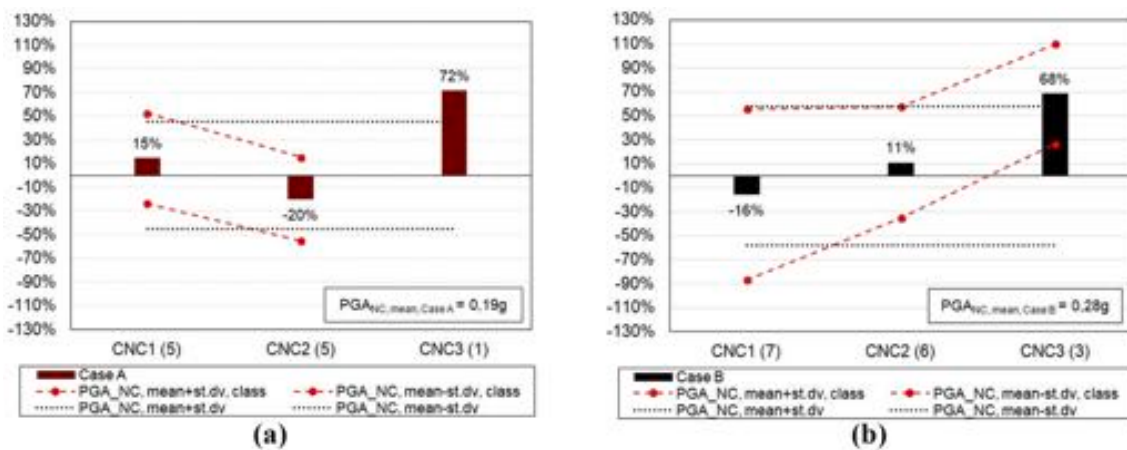

Fig. 21. Differences in NC predictions per limit state criterion for (a) Case A and (b) Case B.

research teams were considered equally valid, since the goal was not to debate the most reliable choices to be adopted. However, the wide variety of choices that analysts have in addressing the seismic assessment of URM existing buildings is evident, leading to very different assessments of the safety. This highlights the need of future research and effort to reduce the arbitrariness in seismic assessment of URM buildings, by providing guidelines for practitioners to make the results from different

procedures consistent.

Declaration of Competing Interest

The authors declare that they have no known competing financial interests or personal relationships that could have appeared to influence the work reported in this paper.

Appendix A. Supplementary data

Supplementary data to this article can be found online at https://doi.org/10.1016/j.istruc.2021.01.096.

References

[1] Lagomarsino S, Cattari S. PERPETUATE guidelines for seismic performance-based assessment of cultural heritage masonry structures. Bull Earthq Eng 2015;13(1):13–47. https://doi.org/10.1007/s10518-014-9674-1.

[2] Cattari S, Lagomarsino S, Bosiljkov V, D'Ayala D. Sensitivity analysis for setting up the investigation protocol and defining proper confidence factors for masonry buildings. Bull Earthq Eng 2015;13(1):129–51. https://doi.org/10.1007/s10518-014-9648-3.

[3] EN 1998-3:2005 Eurocode 8 Design of structures for earthquake resistance - Part 3 Assessment and retrofitting of buildings. Brussels: European Committee for Normalization; 2005.

[4] Cattari S, Camilletti D, Lagomarsino S, Bracchi S, Rota M, Penna A. Masonry Italian code-conforming buildings. Part 2: nonlinear modelling and time-history analysis. J Earthq Eng 2018;22(sup2):2010–40. https://doi.org/10.1080/13632469.2018.1541030.

[5] Manzini CF, Magenes G, Penna A, da Porto F, Camilletti D, Cattari S, et al. Masonry Italian code-conforming buildings. Part 1: case studies and design methods. J Earthq Eng 2018;22(sup2):54–73. https://doi.org/10.1080/13632469.2018.1532358.

[6] D'Altri AM, Sarhosis V, Milani G, Rots J, Cattari S, Lagomarsino S, et al. Modeling strategies for the computational analysis of unreinforced masonry structures: review and classification. Arch Comput Methods Eng 2020;27(4):1153–85. https://doi.org/10.1007/s11831-019-09351-x.

[7] Lagomarsino S, Cattari S. Seismic performance of historical masonry structures through pushover and nonlinear dynamic analyses. In: Ansal A, editor. Perspectives on European Earthquake Engineering and Seismology, Volume 2. Cham: Springer International Publishing; 2015. p. 265–92.

[8] Lemos JV. Assessment of the ultimate load of a masonry arch using discrete elements. In: Presented at the Conference Computer Methods in Structural Masonry. Lisbon, Portugal; 1995.

[9] Roca P, Cervera M, Gariup G, Pela' L. Structural analysis of masonry historical constructions. Classical and advanced approaches. Arch Comput Methods Eng 2010;17(3):299–325. https://doi.org/10.1007/s11831-010-9046-1.

[10] Lourenço PB. Computational strategies for masonry structures.. PhD Thesis. Delft, The Netherlands: Delft University Press; 1996.

[11] Berto L, Saetta A, Scotta R, Vitaliani R. An orthotropic damage model for masonry structures. Int J Numer Meth Eng 2002;55(2):127–57. https://doi.org/10.1002/nme.495.

[12] Lagomarsino S, Penna A, Galasco A, Cattari S. TREMURI program: an equivalent frame model for the nonlinear seismic analysis of masonry buildings. Eng Struct 2013;56:1787–99. https://doi.org/10.1016/j.engstruct.2013.08.002.

[13] Caliò I, Marletta M, Pantò B. A new discrete element model for the evaluation of the seismic behaviour of unreinforced masonry buildings. Eng Struct 2012;40:327–38. https://doi.org/10.1016/j.engstruct.2012.02.039.

[14] Vanin A, Foraboschi P. Modelling of masonry panels by truss analogy – Part 1. Mason Int 2009;22(1):1–10.

[15] Casolo S, Peña F. Rigid element model for in-plane dynamics of masonry walls considering hysteretic behaviour and damage. Earthq Eng Struct Dyn 2007;36(8):1029–48. https://doi.org/10.1002/eqe.670.

[16] D'Asdia P, Viskovic A. Analyses of a masonry wall subjected to horizontal actions on its plane, employing a nonlinear procedure using changing shape finite elements. Trans Model Simul 1995;10:519–26. https://doi.org/10.2495/CMEM950571.

[17] EN 1998-1:2004 Eurocode 8 Design of structures for earthquake resistance - Part 1 General rules, seismic actions and rules for buildings. Brussels: European Committee for Normalization; 2004.

[18] NTC 2018 Updated Technical standards for constructions (Norme Tecniche per le Costruzioni, D.M. 17/01/2018, Ministero delle Infrastrutture e dei Trasporti, S.O. no. 8 alla G.U. del 20/2/2018 no. 42). Rome, Italy; 2018 [in Italian].

[19] New Zealand Society for Earthquake Engineering NZSEE, Structural Engineering Society SESOC, New Zealand Geotechnical Society NZGS, Ministry of Business, Innovation and Employment MBIE, Earthquake Commission EQC Seismic assessment of existing buildings - Section C8 Unreinforced masonry buildings. 2017.

[20] FEMA 356. Pre-standard and commentary for the seismic rehabilitation of buildings. Washington, DC: Federal Emergency Management Agency FEMA; 2000.

[21] Bracchi M, Rota M, Penna A, Magenes G. Consideration of modelling uncertainties in the seismic assessment of masonry buildings by equivalent-frame approach. Bull Earthq Eng 2015;13(11):3423–48. https://doi.org/10.1007/s10518-015-9760-z.

[22] Bartoli G, et al. Epistemic uncertainties in structural modeling: a blind benchmark for seismic assessment of slender masonry towers. J Perform Constr Facil 2017;31(5). https://doi.org/10.1061/(ASCE)CF.1943-5509.0001049.

[23] Magenes G, Lourenço PB, Cattari S. Special Session 18: Seismic modeling of masonry buildings: present knowledge and open challenges for research and practice. Presented at the 16th European Conference on Earthquake Engineering. Thessaloniki, Greece; 2018. [Online] Available: http://www.16ecee.org/programme/special-sessions.

[24] Aşıkoğlu A, Vasconcelos G, Lourenço PB, Pantò B. Pushover analysis of unreinforced irregular masonry buildings: lessons from different modeling approaches. Eng Struct 2020;218. https://doi.org/10.1016/j.engstruct.2020.110830.

[25] Cattari S, et al. A comparative study on a 2-storey benchmark case study through nonlinear seismic analysis. In: Presented at the 16th European Conference on Earthquake Engineering. Thessaloniki, Greece; 2018.

[26] Betti M, Galano L, Vignoli A. Time-history seismic analysis of masonry buildings: a comparison between two non-linear modelling approaches. Buildings 2015;5(2):597–621. https://doi.org/10.3390/buildings5020597.

[27] Marques R, Lourenço PB. Possibilities and comparison of structural component models for the seismic assessment of modern unreinforced masonry buildings. Comput Struct 2011;89(21–22):2079–91. https://doi.org/10.1016/j.compstruc.2011.05.021.

[28] Marques R, Lourenço PB. Benchmarking of commercial software for the seismic assessment of masonry buildings. In: Presented at the International Seminar on Seismic Risk and Rehabilitation of Stone Masonry Housing. Azores, Portugal; 2008.

[29] Galano L, Selleri F. Seismic analysis of masonry buildings: a simplified macro element model (Analisi sismica degli edifici in muratura: un modello semplificato a macroelementi). Ing Sismica 2004;XXI(2):24–45 [in Italian].

[30] McKenna F, Fenves GL, Scott MH. OpenSEES Open System for Earthquake Engineering Simulation. Berkeley: University of California, Pacific Earthquake Engineering Research Centre; 2000.

[31] MIDAS Gen Release 11. MIDAS Information Technology Corporation; 2016.

[32] SAP 2000 Static and Dynamic Finite Element Structural Analysis of Structures Release 18. Berkeley, CA: Computers and Structures Inc. (CSI); 1998.

[33] Displacement analysis finite element software Release 10.2. Delft, The Netherlands; 2000.

[34] ANSYS. Release 11.0. Southpointe, 275 Technology Drive. USA: ANSYS Inc.; 1998.

[35] 3Muri Program. Turin, Italy: S.T.A. DATA S.r.l.; 2018.

[36] Aedes.PCM Design of masonry buildings (Progettazione di Costruzioni in Muratura) Release 2018. AEDES Software for Civil Engineering; 2018 [in Italian].

[37] Magenes G, Remino M, Manzini CF, Morandi P. Bolognini D. SAM II Software for the simplified seismic analysis of masonry buildings; 2006.

[38] 3DMacro 3D computer program for the seismic assessment of masonry buildings (Il software per le murature) Release 1.1103101. Catania, Italy: Gruppo Sismica S.r.l.; 2014 [in Italian].

[39] Lourenço PB, Avila L, Vasconcelos G, Alves JPP, Mendes N, Costa AC. Experimental investigation on the seismic performance of masonry buildings using shaking table testing. Bull Earthq Eng 2013;11(4):1157–90. https://doi.org/10.1007/s10518-012-9410-7.

[40] De Canio G, Dolce M, Goretti A, Marnetto R. Project TREMA - Technologies for the reduction of seismic vulnerability for masonry and reinforced concrete buildings (Tecnologie per la Riduzione degli Effetti sismici sui Manufatti Architettonici in muratura e in c.a.) MURST Legge No. 449/1997, D.M. 10 Maggio 2000; 2000 [in Italian].

[41] Yi T, Moon FL, Leon RT, Kahn LF. Lateral load tests on a two-story unreinforced masonry building. J Struct Eng 2006;132(5):643–52. https://doi.org/10.1061/(ASCE)0733-9445(2006)132:5(643).

[42] Magenes G, Kingsley GR, Calvi GM. Seismic testing of a full-scale, two-story masonry building: test procedure and measured experimental response. In: Rep. 30 - GNDT Exp. Numer. Investig. Brick Mason. Build. Prototype - Numer. Predict. Exp. Univ. Pavia Dep. Struct. Mech.; 1995. https://doi.org/10.13140/RG.2.1.4590.2962.

[43] Augenti N. Seismic design of masonry buildings (Il calcolo sismico degli edifici in muratura). Turin, Italy: UTET; 2004 [in Italian].

[44] Carocci CF, Circo C. Buildings behavior in the urban fabric: the knowledge issue in the post-earthquake reconstruction plans. Key Eng Mater 2014;628:90–5. https://doi.org/10.4028/www.scientific.net/KEM.628.90.

[45] Siano R, Sepe V, Camata G, Spacone E, Roca P, Pelà L. Analysis of the performance in the linear field of equivalent-frame models for regular and irregular masonry

walls. Eng Struct 2017;145:190–210. https://doi.org/10.1016/j.engstruct.2017.05.017.

[46] Circolare 21/01/2019, no. 7 C.S.LL.PP. Instructions for the application of the updated "Technical standards for constructions" (Istruzioni per l'applicazione dell'Aggiornamento delle "Norme tecniche per le costruzioni" di cui al D.M. 17/01/2018). Rome, Italy; 2019 [in Italian].

[47] 3DEC Three-Dimensional Distinct Element Code Release 5.2.. Minneapolis: Itasca Consulting Group Inc.; 1998.

[48] ELS Extreme Loading for Structures 2D & 3D nonlinear static and dynamic structural analysis software. Durham, NC, U.K: Applied Science International LLC; 2018.

[49] LUSAS. Infrastructure analysis and design software Release 15.0. Surrey, UK: Finite Element Analysis Ltd.

[50] Manzini CF, Morandi P, Magenes G, Calliari R. ANDILWall Software for assessment and design of unreinforced, reinforced and mixed masonry buildings - User manual (Software di calcolo e verifica di edifici in muratura ordinaria, armata o mista - Manuale d'uso) Release 2018. Pavia: Università di Pavia, EUCENTRE e CRSoft S.r.l.; 2006 [in Italian].

[51] Meguro K, Tagel-Din H. Applied element method for structural analysis: Theory and application for linear materials. Struct Eng Eng 2000;17(1):21–35.

[52] Malomo D, Pinho R, Penna A. Simulating the shake table response of unreinforced masonry cavity wall structures tested to collapse or near-collapse conditions. Earthq Spectra 2020;36(2):554–78. https://doi.org/10.1177/8755293019891715.

[53] Schreppers GMA, Garofano A, Messali F, Rots JG. DIANA Validation report for Masonry modelling. DIANA FEA report 2016 - DIANA-R1601 and TU Delft Structural Mechanics CiTG Report CM-2016-17; 2017.

[54] EN 338:2009 Structural timber - Strength classes. European Committee for Standardization; 2009.

[55] EN 1992-1-1:2005 Eurocode 2 Design of concrete structures - Part 1-1 General rules and rules for buildings. Brussels: European Committee for Normalization; 2005.

[56] Comité Euro-international du Béton, Fédération Internationale de la Précontrainte CEB-FIP Model Code 1990: Design code Vol. 1993. Thomas Telford Ltd; 1993.

[57] Quagliarini E, Maracchini G, Clementi F. Uses and limits of the equivalent frame model on existing unreinforced masonry buildings for assessing their seismic risk: a review. J Build Eng 2017;10:166–82. https://doi.org/10.1016/j.jobe.2017.03.004.

[58] Dolce M. Schematization and modeling of masonry buildings subjected to seismic actions (Schematizzazione e modellazione degli edifici in muratura soggetti ad azioni sismiche). Ing Delle Costr 1991;25:44–57 [in Italian].

[59] Magenes G, Calvi GM. Cyclic behaviour of brick masonry walls. Presented at the 10th World Conference on Earthquake Engineering. Rotterdam, Netherlands; 1992.

[60] Beyer K, Dazio A. Quasi-static cyclic tests on masonry spandrels. Earthq Spectra 2012;28(3):907–29. https://doi.org/10.1193/1.4000063.

[61] Beyer K, Mangalathu S. Review of strength models for masonry spandrels. Bull Earthq Eng 2013;11(2):521–42. https://doi.org/10.1007/s10518-012-9394-3.

[62] Calderini C, Cattari S, Lagomarsino S. In-plane strength of unreinforced masonry piers. Earthq Eng Struct Dyn 2009;38(2):243–67. https://doi.org/10.1002/eqe.v38:210.1002/eqe.860.

[63] NTC 2008 Technical standards for constructions (Norme Tecniche per le Costruzioni, D.M. 14/01/2008, Ministero delle Infrastrutture e dei Trasporti, S.O. no. 30 to the G.U. on 04/02/2008 no. 29). Rome, Italy; 2008 [in Italian].

[64] Vanin F, Zaganelli D, Penna A, Beyer K. Estimates for the stiffness, strength and drift capacity of stone masonry walls based on 123 quasi-static cyclic tests reported in the literature. Bull Earthq Eng 2017;15(12):5435–79. https://doi.org/10.1007/s10518-017-0188-5.

[65] Knox CL. Assessment of perforated unreinforced masonry walls responding in-plane. PhD Thesis. Auckland, New Zealand: Department of Civil and Environmental Engineering, University of Auckland, Auckland; 2012.

[66] Vanin F, Penna A, Beyer K. Equivalent-frame modeling of two shaking table tests of masonry buildings accounting for their out-of-plane response. Front Built Environ 2020;6:42. https://doi.org/10.3389/fbuil.2020.00042.

[67] Turnšek V, Čačovič F. Some experimental results on the strength of brick masonry walls. In: Presented at the 2nd International Brick Masonry Conference, Stoke-on-Trent, UK; 1971, pp. 149–56.

[68] Giuffrè A. Vulnerability of historical cities in seismic areas and conservation criteria. In: Presented at the Conference Earthquakes and Residential Housing (Terremoti e Civiltà Abitative). Italy; 1995.

[69] Heyman J. The stone skeleton. Int J Solids Struct 1966;2(2):249–79. https://doi.org/10.1016/0020-7683(66)90018-7.

[70] Di Michele F, Cantagallo C, Spacone E. Effects of the vertical seismic component on seismic performance of an unreinforced masonry structures. Bull Earthq Eng 2020; 18(4):1635–56. https://doi.org/10.1007/s10518-019-00765-3.

[71] Liberatore D, Doglioni C, AlShawa O, Atzori S, Sorrentino L. Effects of coseismic ground vertical motion on masonry constructions damage during the 2016 Amatrice-Norcia (Central Italy) earthquakes. Soil Dyn Earthq Eng 2019;120: 423–35. https://doi.org/10.1016/j.soildyn.2019.02.015.